5. SITE 736[1]

Shipboard Scientific Party[2]

HOLE 736A

Date occupied: 25 December 1987

Date departed: 28 December 1987

Time on hole: 2 days, 4 hr, 45 min

Position: 49°24.12′S, 71°39.61′E

Bottom felt (rig floor: m, drill-pipe measurement): 639.5

Distance between rig floor and sea level (m): 10.5

Water depth (drill-pipe measurement from sea level, m): 629.0

Total depth (rig floor, m): 891.8

Penetration (m): 252.3

Number of cores: 30

Total length of cored section (m): 250.3

Total core recovered (m): 147.05

Core recovery (%): 58

Oldest sediment cored:
Depth sub-bottom (m): 242.6
Nature: diatom ooze
Earliest age: late Pliocene
Measured velocity (km/s): 1.53

HOLE 736B

Date occupied: 28 December 1987

Date departed: 28 December 1987

Time on hole: 1 hr, 30 min

Position: 49°24.12′S, 71°39.61′E

Bottom felt (rig floor: m, drill-pipe measurement): 638.6

Distance between rig floor and sea level (m): 10.5

Water depth (drill-pipe measurement from sea level, m): 628.1

Total depth (rig floor, m): 666.0

Penetration (m): 27.4

Number of cores: 3

Total length of cored section (m): 27.4

Total core recovered (m): 27.81

Core recovery (%): 101

Oldest sediment cored:
Depth sub-bottom (m): 27.4
Nature: diatom ooze, diatom ooze with volcanic detritus, and sand
Earliest age: Quaternary
Measured velocity (km/s): 1.44

HOLE 736C

Date occupied: 28 December 1987

Date departed: 29 December 1987

Time on hole: 1 day, 2 hr, 15 min

Position: 49°24.16′S, 71°39.65′E

Bottom felt (rig floor: m, drill-pipe measurement): 639.5

Distance between rig floor and sea level (m): 10.5

Water depth (drill-pipe measurement from sea level, m): 629.0

Total depth (rig floor, m): 1010.5

Penetration (m): 371.0

Number of cores: 18

Total length of cored section (m): 371.0

Total core recovered (m): 77.41

Core recovery (%): 20

Oldest sediment cored:
Depth sub-bottom (m): 371.0
Nature: diatom ooze
Earliest age: late early Pliocene
Measured velocity (km/s): 1.46

Principal results: Site 736 (49°24.12′S, 71°39.61′E; target Site KHP-1) is on the northern part of the Kerguelen-Heard Plateau in a water depth of 629 m. A 371-m-thick continuous section of upper Pliocene and Quaternary diatomaceous ooze with a varying component of volcanic ice-rafted and/or detrital material was cored in three holes at the site.

Coring commenced on 26 December 1987 in Hole 736A with the advanced piston corer (APC). With the exception of the interval between 119.5 and 146.4 m below seafloor (mbsf), which was cored with the extended core barrel (XCB), APC coring was completed in the upper 165.4 m of the sediment column with an average recovery of 94%. Below that level, XCB coring in Hole 736A continued until 242.6 mbsf, where poor recovery and drilling characteristics resulted in the decision to switch to rotary core barrel (RCB) coring. Hole 736B was a shallow APC site that duplicated coring in the upper 27 m of Hole 736A in order to allow a more complete recovery of the uppermost Quaternary. In Hole 736C, RCB coring commenced at 206.9 mbsf and continued to a total depth of 371 mbsf on 29 December. Recovery was variable, ranging from no recovery to full recovery and averaging 47%.

Two lithologic units were recognized at Site 736. The upper 257 m of the section consists of diatomaceous ooze containing scattered pebbles and gravels that appear to be ice rafted. The age of the base of this unit is approximately 2.6 Ma according to diatom stratigraphy, so the base of the unit probably is tied with the onset of ice rafting in the area. Approximately this same upper unit (0–260 mbsf) is characterized on the seismic lines by closely spaced strong reflectors. Regionally, considerable channeling and thickness variations are associated with this upper unit, which appears to be unit S1 of Munschy and Schlich (1987). Below 257 mbsf diatomaceous oozes continue (Unit II) without appreciable detrital content to the base of the hole (371 mbsf).

Diatoms and radiolarians are common and consistent in the Site 736 sediments, and standard Antarctic zonations can be applied. Coring at the site was terminated in the diatom *Nitzschia interfrigidaria/Coscinodiscus vulnificus* Zone (3.1–3.4 Ma). Carbonate

[1] Barron, J., Larsen, B., et al., 1989. *Proc. ODP, Init. Repts.*, 119: College Station, TX (Ocean Drilling Program).

[2] Shipboard Scientific Party is as given in the list of Participants preceding the contents.

is sparse and sporadic in its occurrence. Biostratigraphy indicates that the section is complete, with sediment-accumulation rates ranging between 54 and 140 m/m.y. Unfortunately, the magnetic signal of the sediments is weak, and no reversal stratigraphy could be established.

No gas was found in Site 736 sediments, and total organic carbon is low.

BACKGROUND AND OBJECTIVES

Paleoceanography

The Antarctic Circumpolar Current (ACC) is a major surface current that is driven by strong westerly winds and circles the Antarctic continent between the latitudes of 40° and 65°S. Barker and Burrell (1982) suggested that the ACC first developed in the earliest Miocene and that progressive polar cooling, which typified the late Cenozoic, resulted from a successive strengthening of the ACC and increasing thermal isolation of Antarctica. Near the axis of the ACC, the Antarctic Convergence, or Polar Front, separates subantarctic waters to the north from antarctic waters to the south (Gordon, 1971). The Antarctic Convergence also approximates the boundary between calcareous oozes to the north and biosiliceous oozes to the south (Barker and Burrell, 1982). The biosiliceous oozes, which circle Antarctica in a broad band between about 45° and 65°S, are the major pelagic sediment type that typifies the modern Southern Ocean.

Site 736 (49°24.12′S, 71°39.61′E), the northern site of the Kerguelen Plateau paleoceanographic transect, lies beneath the modern Antarctic Convergence in 629 m of water; the convergence, however, may migrate seasonally through as much as 4° of latitude according to Gordon (1971). A major objective of paleoceanographic studies at Site 736 was to trace the movement of the Antarctic Convergence through time, both with sediment types and with microfossil assemblages. We believe that climatic fluctuations during the Neogene should be reflected by northward and southward displacement of the Antarctic Convergence across Site 736, resulting in the alternating appearance of antarctic and temperate assemblages in the sediments.

Kemp et al. (1973) used sedimentary evidence from Deep Sea Drilling Project (DSDP) Leg 28 to suggest that the Antarctic Convergence moved northward to its present location at the beginning of the Pliocene. Similarly, Brewster's (1980) argument that biosiliceous sediment-accumulation rates in the Southern Ocean increased dramatically in the earliest Pliocene is further evidence supporting a northward movement of the convergence and expansion of the Antarctic surface-water mass. Ciesielski and Grinstead (1986) provided more detail on numerous shifts in position of the Antarctic Convergence (Polar Front) in the southwest Atlantic during the middle to late Pliocene. We hoped to carry out similar studies at Site 736.

Site 736's location on the Kerguelen Plateau, above the regional carbonate compensation depth (CCD), suggests that carbonate should also be present in the Neogene sediments to be recovered there. Nearby emergent areas on Kerguelen and Heard islands also are likely to contribute detrital sediments and scattered ash. Indeed, piston cores collected by the French research vessel *Marion Dufresne* reveal that Neogene sediments are diatomaceous muds with consistent, but variable, detrital components of volcanic origin and minor amounts of carbonate (R. Schlich and L. Leclaire, pers. comm., 1987).

Regional Geology and Geophysics

The Kerguelen-Heard Plateau has been studied by American, French, Australian, and Soviet research ships (see references in Munschy and Schlich, 1987). The data collected consist of bathymetry, seismic reflection, sonobuoy wide-angle reflection and refraction, dredges, piston cores, gravimetry, and magnetics. The recent article by Munschy and Schlich (1987) summarized the present knowledge of the area (see "Introduction" chapter, this volume).

Munschy and Schlich (1987) divided the Neogene sequence on the Kerguelen-Heard Plateau into two units, S1 and S2. The younger sequence, S1, exists only in the central part of the plateau and shows considerable variations in thickness. Unit S2, the older Neogene sequence, is found over the entire plateau and also shows significant variations in thickness. Site 736 was chosen on French seismic line MD 26-10 at shotpoint 2300 (Munschy and Schlich, 1987) in order to maximize the thickness of Neogene sequences S1 and S2.

Interpretation of the seismic stratigraphy suggests that as much as 910 m of Neogene section (units S1 and S2) lies above a regional middle Tertiary unconformity (discordance A of Munschy and Schlich, 1987) at Site 736. Discordance A is a major event in the sedimentary section, which probably marks a hiatus separating the middle Eocene carbonates from the lower Miocene diatomaceous muds or clastic deposits, according to Munschy and Schlich (1987). Munschy and Schlich (1987) interpret discordance A to be the time of uplift and rifting of the combined Kerguelen-Heard Plateau and Broken Ridge. This event, therefore, should separate the pre-rifting from breakup and post-breakup sequences; presumably, the area of Site 736 was subaerially exposed between the middle Eocene and the early Miocene.

Objectives

The expanded Neogene section expected at Site 736 should be an excellent stratigraphic section of high-resolution biostratigraphic and paleoceanographic studies. In addition, a second objective at Site 736 was to date the reflector at 910 mbsf, which should correspond with discordance A of Munschy and Schlich (1987). Inasmuch as seismic units S1 and S2 show considerable regional variations in thickness, we planned to study the sediment properties in order to determine depositional processes. Recovery of the pre-rift Eocene carbonates could provide an important northern point on the Ocean Drilling Program (ODP) Legs 119 to 120 north-south paleoceanographic transect for the pre-Neogene. Additionally, these sediments should compare well with Eocene sediments to be cored on Broken Ridge during ODP Leg 121.

SITE GEOPHYSICS

Site 736 was proposed based on multichannel seismic-reflection (MCS) lines collected by *Marion Dufresne* (MD 26-10, shotpoint 2300, and MD 26-04) and supplemented by single-channel seismic-reflection data from USNS *Eltanin* collected in 1971. On approach to the site (ODP line 119-01), a 30-nmi-long geophysical survey line with standard navigation, seismic, and magnetic equipment (see "Explanatory Notes" chapter, this volume) was recorded by *JOIDES Resolution* parallel to MD 26-04 and across *Eltanin* lines 26 and 15 from 49°5.45′S, 71°27.0′E to 49°33.05′S, 71°45.0′E. The survey line passed over the target site (Fig. 1), providing a good tie of drilling data to regional geophysical surveys.

A sonobuoy was deployed about 1 km before the target site and was recorded for 20 km to the end of the survey line. A beacon was dropped about 2.5 km beyond the target site to avoid drilling into a subsurface anticlinal structure. At the end of the survey line, the ship turned to a reciprocal course and returned to the beacon. The final choice for Site 736 (49°24.12′S, 71°39.61′E) was about 1.5 km south of the target site (1 km from the beacon) to avoid possible buried channel deposits where the beacon was dropped. A second beacon was dropped to mark Site 736.

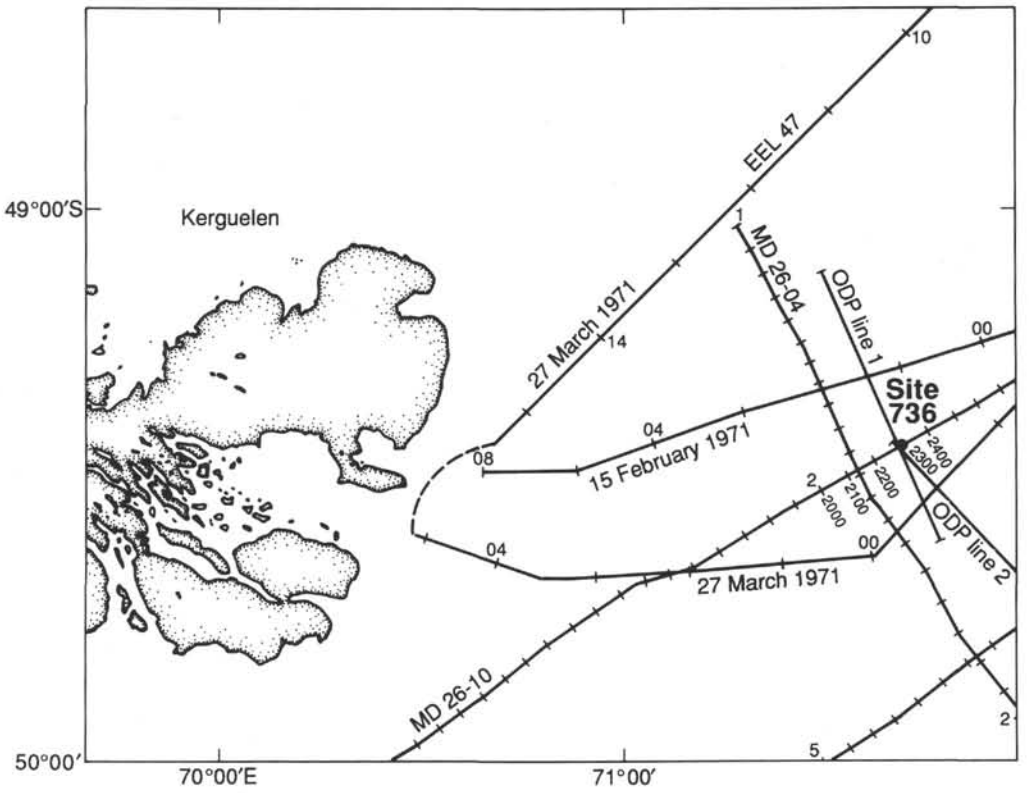

Figure 1. Index map of seismic lines recorded during site surveys for Site 736.

Sonobuoy Data

The sonobuoy was deployed 1 km from the proposed site to acquire velocity data using wide-angle reflection and refraction arrivals through the shallow sedimentary section directly below the site (Fig. 2). Strong direct, reflection, and refraction arrivals were recorded over the first 6 km of the sonobuoy station. These recorded arrivals provided good estimates of interval and refraction velocities for the sedimentary section and acoustic basement (refraction velocity only) (Fig. 3). Velocities computed from the sonobuoy were used prior to drilling to estimate depths for seismic-reflection horizons beneath Site 736. This preliminary velocity-depth information was used extensively for guiding the drilling strategy (Table 1).

Seismic-reflection data across Site 736 indicate that the shallow sedimentary section (above 1.9 s; EE, Fig. 3) contains an upper well-layered unit and a lower acoustically-transparent unit with scattered reflectors. The sonobuoy data, however, show strong continuous reflections throughout both units, thereby providing good reflections (AA to FF) for interval-velocity estimates. Interval velocities are low (1.45–1.79 km/s) within both units (Fig. 4). The velocity increase with depth is probably due to burial compaction of the predominately diatomaceous sedimentary section. The absence of identifiable refraction arrivals from horizons AA and BB, as well as the large horizontal offset to slow (1.5 and 1.6 km/s) refraction arrivals (probably from layers CC and DD; Table 1), also suggests that velocities are less than 1.8 km/s in the upper part of the sedimentary section (i.e., above at least 846 mbsf, horizon EE).

Abrupt velocity increases occur at both horizons EE and FF, which are associated with linear refraction arrivals with velocities of 2.96 and 3.35 km/s, respectively. These horizons were not reached by drilling at Site 736; however, the velocities are similar to those for sedimentary rocks drilled at Site 737 (see "Site Geophysics" section, "Site 737" chapter, this volume). At Site 737, calcareous claystone and chert-limestone were recovered from units with distinct refraction velocities of 2.52 and 3.7–3.9 km/s (sonobuoy units DD-EE and EE-FF, respectively).

Refraction velocities for likely igneous or massive volcanic rocks (e.g., greater than 4.5 km/s) were not recorded in the first sonobuoy at Site 736; however, they were recorded at Site 737, where 794 m of 3.7–3.9-km/s rocks overlies likely igneous basement (4.51 km/s). The approximate total thickness of strata above horizon FF at Site 736 is 2037 m (Table 1). If rocks between horizon FF and igneous basement are of equivalent thickness to those at Site 737 (e.g., 794 m), then the total sedimentary section at Site 736 would be 2785 m. This thickness is probably a minimum value, because the seismic-reflection data between Sites 736 and 737 indicate that the sedimentary section thickens toward Site 737.

The sonobuoy interval velocities are similar to those determined from routine analysis of stacking velocities for MCS line MD 26-10 near Site 736. The sonobuoy data provide more complete velocity information than MCS data because the greater horizontal offset of the sonobuoy (up to 5 km) provides additional refraction-velocity information concerning velocity gradients and velocity discontinuities.

OPERATIONS

The expedition began on 14 December 1987 at Port Louis, Mauritius.

Mauritius Port Call

Leg 119 began with the first mooring line at Berth 5, Port Louis Harbor, at 0615 hr, 14 December. The major port call activities were logistical with large shipments of ODP cores and special drilling/coring equipment from Leg 118 to be off-loaded. The oncoming shipments for the Antarctic voyage were larger

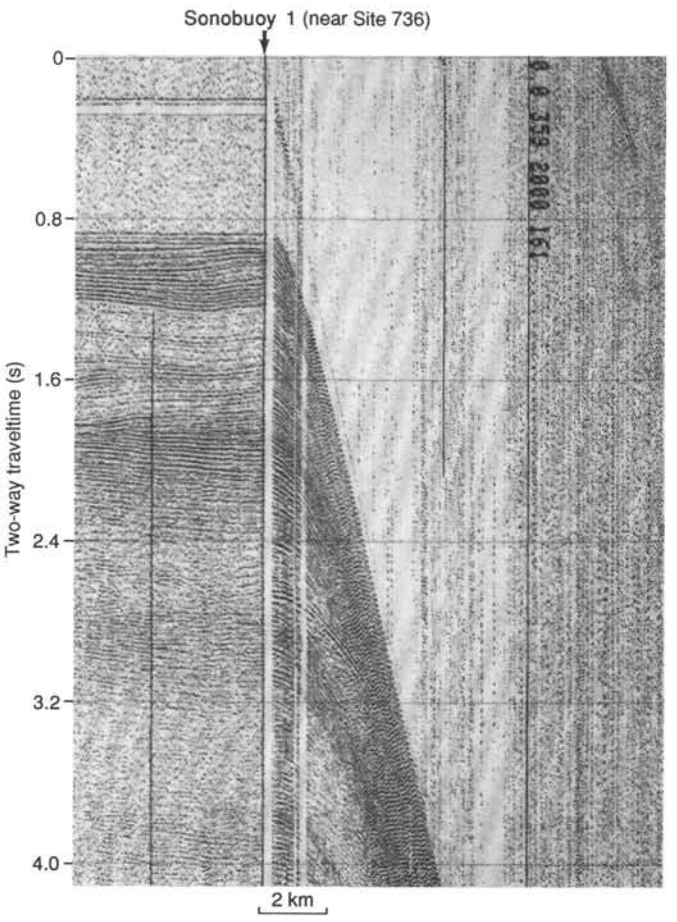

Figure 2. Vertical-incident seismic and sonobuoy seismic record for sonobuoy station 1. Site 736 is about 2 km south of where the sonobuoy was deployed. See Figure 1 for location.

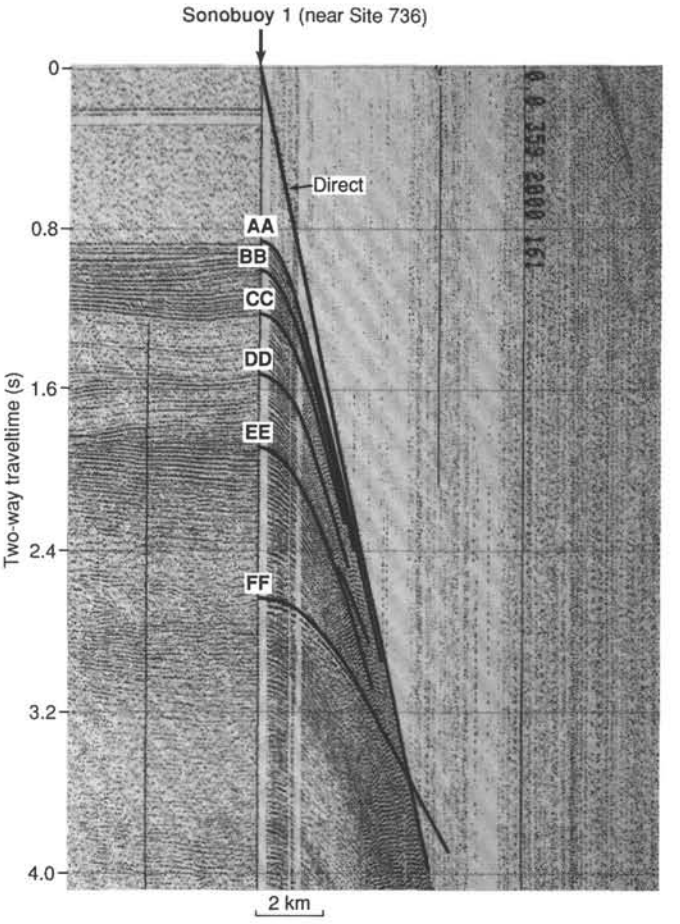

Figure 3. Vertical-incident seismic and sonobuoy seismic record for Site 736 showing wide-angle reflection and refraction interpretations. Letters denote layers in Table 1. See Figure 1 for location.

than normal, and a considerable amount of freight was backloaded from local storage in Mauritius. Other work items included the annual American Bureau of Shipping inspection for the ship; repair of number 7 engine and number 2 crane; repair of cracks in the thruster wells; loading of drill water, lube oil, and 900 metric tons of fuel; and UDI and ODP crew changes.

On the morning of 18 December, the vessel had to shift two berths down the wharf to accommodate another ship. Loading then continued until minutes before the last line was cast off at 1730 hr.

Mauritius to Site 736

Generally good weather prevailed during the scheduled eight-day transit to Kerguelen. Winds were light to moderate and usually from astern. With the help of a following current, an average speed of 11.7 kt was achieved for the first four days. On 22 December the Southern Ocean greeted *JOIDES Resolution* with beam winds gusting to 45 kt. The swell built to 7 m, and the vessel experienced rolls to 20°. Speed dropped briefly below 10 kt, but conditions moderated after about a day. Following winds then returned and assisted the ship into colder waters before they shifted to the south and impeded progress somewhat.

The drill site, which is about 40 nmi east of Kerguelen Island, was approached from the north, and seismic profiling gear was streamed about 18 nmi north of the site. Speed was reduced to 6 kt to improve record quality. At about 2 nmi north of the site, a sonobuoy was deployed for a seismic-refraction velocity profile. A recoverable positioning beacon was launched on the first pass over the location. The profile was then extended beyond the drop point before the vessel returned on a reciprocal course and recrossed the beacon location. The profiling gear was recovered, and the vessel took station on the beacon. As preparations were made for the pipe trip, the drilling position

Table 1. Preliminary results for sonobuoy 1, Site 736.

Horizon[a]	Vrms (km/s)	Vint (km/s)	Ti (s)	Zi (km)	Vrfr (km/s)	To (s)
AA	1.465	1.45	0.87	0.628	nr	—
BB	1.463	1.56	1.04	0.751	nr	—
CC	1.479	1.56	1.24	0.907	[b]1.5	0.35
DD	1.496	1.79	1.53	1.133	[b]1.6	0.68
EE	1.566	3.22	1.91	1.474	2.96	1.57
FF	2.159	—	2.65	2.665	3.35	1.88

Note: Vrms = rms velocity for horizon; Vint = interval velocity computed using Vrms, Ti, and Dix equation (e.g., Vint between horizons EE and FF is 3.22 km/s); Ti = vertical incidence reflection time (two-way) to horizon; Zi = total depth from sea level to horizon computed from Vint and Ti (water depth = 628 m); Vrfr = refraction velocity associated with horizon (e.g., Vrfr at top of layer CC-DD is 1.5 km/s); To = intercept time for refractor associated with horizon; nr = no refractor observed.

[a] Letters of horizons do not correlate between drill sites and do not correspond to prior stratigraphic analyses.

[b] Refractors assumed to be associated with the horizon.

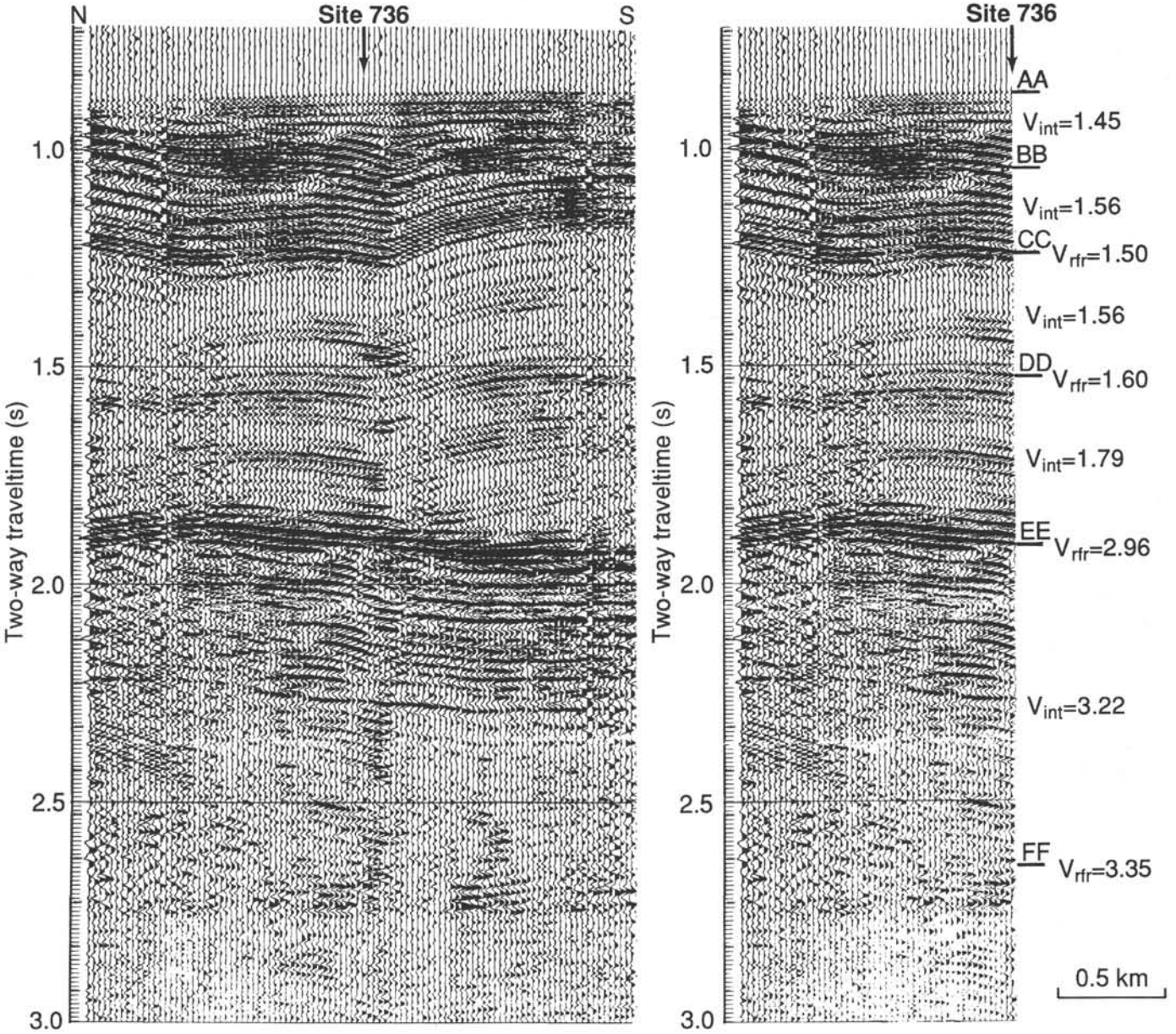

Figure 4. Vertical-incident seismic data showing sonobuoy interval and refraction velocities, Site 736.

was refined by offsetting the ship 1000 m to the north and launching a second beacon.

The total transit/survey distance of 1943 nmi was covered at an average speed of 11.0 kt.

Site 736—Kerguelen-Heard Plateau

Hole 736A

Operations began slowly, with temperatures of 3° to 4°C and winds gusting to 45 kt. Bottom-hole assemblies (BHA) were constructed, and all components were measured and checked for internal clearance. After an electrical problem in the top drive was resolved, Hole 736A was spudded at 1800 hr on 26 December 1987 at a depth of 629 m by drill-pipe measurement.

APC cores were taken from the seafloor to 117.5 mbsf (Table 2) before pull-out force reached 60,000 lb. Extreme vessel motion resulted in short APC stroke, failed core liners, and sheared overshot pins. On one occasion the coring line failed about 20 m above the coring assembly. It was successfully recovered from the drill string, along with the full core barrel, using a wireline-deployed barbed spear. Oriented APC and heatflow probe runs were only partially successful because of vessel motion conditions.

Three XCB cores (119-736A-17X through 119-736A-19X, 117.5 to 146.4 mbsf) were then attempted, but recovery was poor in the soft diatom ooze. The APC corer was redeployed, and two more successful APC cores (119-736A-20H through 119-736A-21H, 146.4 to 165.4 mbsf) were recovered before the system survived a 130,000-lb pull-out. XCB coring continued, with recovery of only about 20%, to 252.3 mbsf. Minor amounts of basalt and pumice gravel continued to fall from an uphole source and to be recovered at the top of each core, but the gravel did not adversely affect operations.

Because the ultimate coring objective at Site 736 was in excess of 900 mbsf and hard sedimentary rocks were expected, Hole 736A was terminated to change the BHA. That step had been planned for deeper in the section, but the low core recovery rendered further XCB coring a waste of time.

Table 2. Coring summary, Site 736.

Core no.	Date (Dec. 1987)	Time	Depth top (mbsf)	Depth bottom (mbsf)	Length cored (m)	Length recovered (m)	Recovery (%)
119-736A-							
1H	26	1810	0.0	9.0	9.0	8.95	99.4
2H	26	1850	9.0	18.5	9.5	5.31	55.9
3H	26	2100	18.5	28.0	9.5	6.31	66.4
4H	26	2145	28.0	33.0	5.0	4.96	99.2
5H	26	2300	33.0	38.0	5.0	5.20	104.0
6H	27	0000	38.0	43.0	5.0	4.52	90.4
7H	27	0045	43.0	48.0	5.0	5.21	104.2
8H	27	0115	48.0	53.0	5.0	5.32	106.4
9H	27	0145	53.0	59.0	6.0	5.99	99.8
10H	27	0230	59.0	68.5	9.5	7.35	77.3
11H	27	0300	68.5	73.5	5.0	4.78	95.6
12H	27	0615	73.5	79.5	6.0	5.96	99.3
13H	27	0700	79.5	89.0	9.5	9.76	103.0
14H	27	0830	89.0	98.5	9.5	9.87	104.0
15H	27	0915	98.5	108.0	9.5	9.47	99.7
16H	27	0950	108.0	117.5	9.5	9.70	102.0
17X	27	1100	119.5	127.1	7.6	1.38	18.1
18X	27	1115	127.1	136.8	9.7	0.87	9.0
19X	27	1300	136.8	146.4	9.6	1.64	17.1
20H	27	1405	146.4	155.9	9.5	8.40	88.4
21H	27	1600	155.9	165.4	9.5	9.06	95.3
22X	27	1755	165.4	175.0	9.6	0.65	6.8
23X	27	1830	175.0	184.6	9.6	3.36	35.0
24X	27	1900	184.6	194.4	9.8	2.19	22.3
25X	27	1930	194.4	203.9	9.5	0.04	0.4
26X	27	2015	203.9	213.5	9.6	5.75	59.9
27X	27	2240	213.5	223.2	9.7	1.26	13.0
28X	27	2315	223.2	232.9	9.7	0.00	0.0
29X	28	0045	232.9	242.6	9.7	3.22	33.2
30X	28	0130	242.6	252.3	9.7	0.57	5.9
					250.3	147.05	
119-736B-							
1H	28	0925	0.0	8.4	8.4	8.33	99.1
2H	28	0950	8.4	17.9	11.0	9.86	89.6
3H	28	1010	17.9	27.4	9.5	9.62	101.0
					28.9	27.81	
119-736C-							
1W	29	0030	0.0	206.9	206.9	0.10	
2R	29	0100	206.9	216.5	9.6	3.03	31.5
3R	29	0130	216.5	226.0	9.5	0.00	0.0
4R	29	0320	226.0	235.7	9.7	0.23	2.4
5R	29	0405	235.7	245.4	9.7	6.27	64.6
6R	29	0445	245.4	255.0	9.6	0.10	1.0
7R	29	0515	255.0	264.7	9.7	2.36	24.3
8R	29	0550	264.7	274.4	9.7	2.85	29.4
9R	29	0630	274.4	284.0	9.6	9.86	103.0
10R	29	0700	284.0	293.7	9.7	9.66	99.6
11R	29	0735	293.7	303.4	9.7	6.43	66.3
12R	29	0805	303.4	313.1	9.7	0.57	5.9
13R	29	0835	313.1	322.8	9.7	9.56	98.5
14R	29	0910	322.8	332.4	9.6	4.49	46.8
15R	29	0945	332.4	342.0	9.6	9.74	101.0
16R	29	1010	342.0	351.6	9.6	5.51	57.4
17R	29	1045	351.6	361.3	9.7	1.82	18.7
18R	29	1130	361.3	371.0	9.7	4.83	49.8
(Coring)					164.1	77.31	
(Washing)					206.9	0.10	
					371.0	77.41	

Hole 736B

Because of adverse weather and a core liner failure, the uppermost sediments were incompletely recovered in Hole 736A. A second effort was made to recover the valuable material lost when the bit cleared the seafloor after abandonment of Hole 736A. Three quick APC cores were taken from the seafloor (water depth of 628 m) to a depth of 28.9 mbsf with a recovery of 27.8 m. Under much-improved weather conditions, complete core recovery was achieved. A round trip was then made for the RCB BHA.

Hole 736C

Following the pipe trip, the soft upper sediments were washed to a depth of 207 mbsf. The hole was flushed with drilling mud, and a successful heatflow-probe measurement was taken.

Continuous RCB coring then began, with results equivalent to those with the XCB through the repeated interval. The sediment became somewhat firmer with depth, and the recovery rate improved to about 65%.

When 371 m of fairly uniform ooze had been penetrated, revealing an extremely high rate of sedimentation (~140 m/m.y.), the drilling objectives of the site were re-evaluated (see "Background and Objectives" section, "Site 737" chapter). We determined that the desired scientific results could be achieved more efficiently by terminating operations at Site 736 and moving to nearby target Site KHP-3, where the younger sediment section was thinner or absent.

Hole 736C was filled with weighted mud and abandoned. The drill string was recovered, and the drillship departed Site 736 at 1630 hr on 29 December.

LITHOSTRATIGRAPHY AND SEDIMENTOLOGY

The sediment sequence drilled at Site 736 has been divided into two lithologic units: Unit I is a diatom ooze containing substantial basaltic volcanic debris and more than 0.5% organic carbon; Unit II is a diatom ooze containing minor feldspathic and pumiceous detritus, nannofossil ooze, and less than 0.4% organic carbon. The divisions are summarized in Table 3 and Figure 5. Smear slide compositional data for the units are included in the barrel sheets. In addition to examination of the smear slides and of the mineralogy of the sand fraction as observed through the binocular microscope, six samples were analyzed by X-ray diffraction (XRD). Carbonate analyses were conducted on the core-catcher samples ("Inorganic Geochemistry" section, this chapter). Grain-size analysis was made using a Lasentech Lab-Tec 100 scanning-laser particle-size analyzer ("Explanatory Notes" chapter). Coarse-sediment fractions were examined visually.

Drilling Deformation

Much of the core was disturbed during coring. The sediment is soft to sightly firm; the latter was affected by closely spaced, concave-up bowed partings. A particular problem experienced at this site was drill hole cave-in contamination of the upper part of the APC cores. Discrimination of these artifact graded gravels from *in-situ*, natural graded gravel was based on criteria described in the "Explanatory Notes" chapter. Contaminated intervals occurred in Sections 119-736A-4H-1, 0–30 cm, 119-736A-5H-1, 0–57 cm, 119-736A-6H-1, 0–75 cm, 119-736A-7H-1, 0–50 cm, 119-736A-8H-1, 0–37 cm, 119-736A-9H-1, 0–35 cm, 119-736A-10H-1, 0–?150 cm, 119-736A-11H-1, 0–37 cm, 119-736A-12H-1, 16–90 cm, 119-736A-13H-1, 0–57 cm, 119-736A-14H-1, 0–55 cm, 119-736A-15H-1, 0–57 cm, 119-736A-16H-1, 0–12 cm, 119-736A-17X-1, 0–18 cm, 119-736A-18X-1, 0–47 cm, 119-736A-18X-CC, 0–41 cm, 119-736A-19X-1, 0–151 cm, 119-736A-19X-CC, 0–14 cm, 119-736A-20H-1, 0–56 cm, 119-736A-21H-1, 0–32 cm, 119-736A-22X-1, 0–39 cm, 119-736A-22X-CC, 0–26 cm, 119-736A-24X-1, 0–66 cm, 119-736A-27X-1, 0–10 cm, 119-736A-29X-1, 0–4 cm, 119-736A-30X, 0–57 cm, 119-736C-2R-1, 0–12 cm, 119-736C-4R-1, 0–12 cm, (?)119-736C-13R-1, 0–10 cm, and (?)119-736C-18R-1, 0–~15 cm. However, no agreement was reached on whether Sections 119-736A-6H-1, 75–90

Table 3. Summary of lithologic units, Site 736.

Age	Unit	Depth (mbsf)	Thickness (m)	Core interval	Dominant lithologies
Quaternary–late Pliocene	I	0–257.1	257.1	736A-1H to -30X-CC 736B-1H to -3H-CC 736C-2R to -7R-2, 27 cm	Diatom ooze with minor volcanic debris
late Pliocene	II	257.1–366.1	109.0	736C-7R-2, 27 cm, to -18R-4	Diatom ooze with minor nannofossil ooze

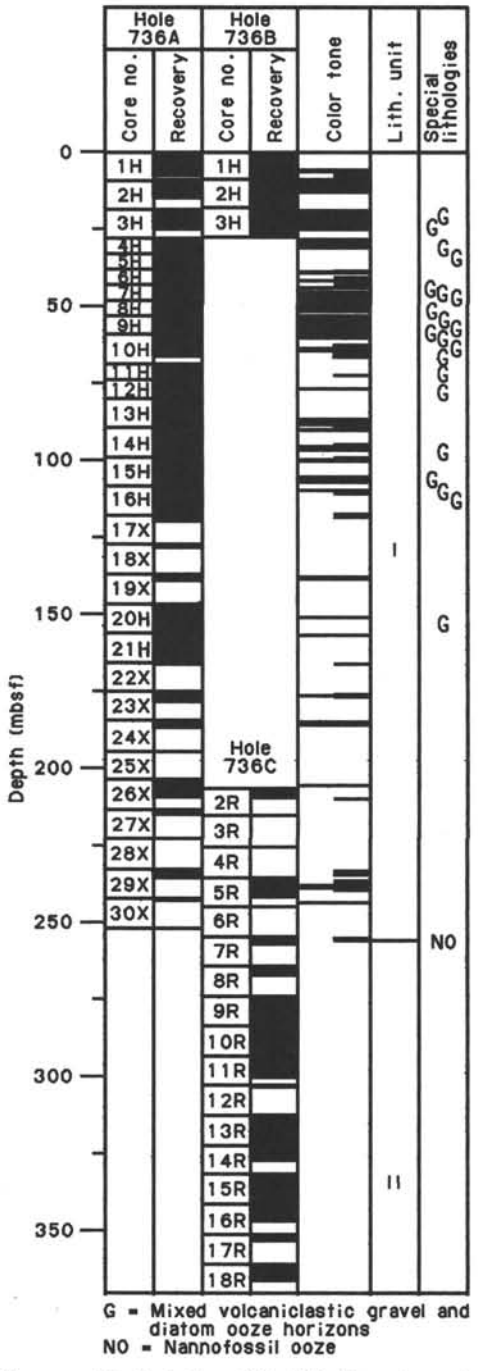

Figure 5. Summary lithologic log at Site 736. The color variation plotted is an indication of volcanic content. Darker colors (longer lines) indicate a greater content of volcanic material.

cm, and 119-736A-7H-1, 0–50 cm, are downfall material or *in-situ* gravels. A problem that remains in regarding all these as contaminants is that their source layers were not sampled at shallower levels in the hole, despite almost complete recovery in the initial cores.

The soupy nature of the sediment throughout Hole 736C is a result of remobilization during rotary drilling. Drilling disturbance data are summarized in the barrel sheets. Otherwise, drilling deformation features are similar to those encountered at other ODP sites.

Lithostratigraphy

Unit I

Diatom ooze with minor volcanic debris

Core 119-736-1H through Sample 119-736A-6H-1, 75 cm; depth, 0–257.1 mbsf.
Core 119-736B-1R through Section 119-736B-3H-CC; depth, 0–27.4 mbsf.
Core 119-736C-2R through Sample 119-736C-7R-2, 61 cm; depth, 0–257.1 mbsf.
Age: Quaternary–late Pliocene.

Unit I is composed of diatom oozes with varied degrees of incorporated volcanic detritus, minor tuffs, and basaltic gravels recovered mainly in the form of downhole cave-in contamination.

The unit consists of olive-colored (e.g., 5Y 4/3) diatom ooze, interstratified with darker olive gray (e.g., 5Y 4/2) to gray-black (e.g., 5Y 3/1) diatom ooze. The darker varieties bear disseminated volcanic silt, sand, gravel, and clay. The amounts of volcanic detritus incorporated range up to 15%; the colors gray black (5Y 3/1, 3/2, 2.5/1, and 2.5/2), olive gray (5Y 4/1, 4/2, 5/1, and 5/2), and olive (5Y 4/3, 4/4, 5/3, 5/4, and 5/6) represent diatom oozes with high, moderate, and low volcanic detrital content, respectively. Figure 5 illustrates trends in color tones through Unit I, suggesting that volcanic incorporation tends to increase to the top of the sequence. The base of Unit I is taken as the lowermost olive gray (5Y 4/2) or darker olive diatom ooze (257.1 mbsf at 27 cm in Section 119-736C-7R-2; see Fig. 5) signifying the onset of volcanic contribution to the diatom ooze.

Grain-size analyses of the oozes indicate that all but a few of the pure and impure diatom oozes are of silty texture with 1%–7% sand, 82%–88% silt, 11%–17% clay fraction, and 10–14-μm mean grain size. The clay-size fraction contains at least some broken diatom material. The silt and sand fractions consist largely of entire or fragmented diatoms. Organic carbon contents are between 0.5% and 1.5%, whereas carbonate values are generally 0%–4%, ranging to 10% (see "Organic Geochemistry" section, this chapter; Fig. 6). From smear slide examinations 75%–100% of the sediments consists of diatoms, 0%–20% is clay minerals, and 0%–12% is volcanic glass. Other minor components include nannofossils and foraminifers.

For the most part, the diatom ooze sediments are thick bedded (usually 0.5 to 4 m) and internally homogeneous, apart

from a few slight and vague color changes. Bedding relations between the color tone variations are not clear. Most lithologic boundaries are diffuse, irregular, and/or wispy, and many are steeply inclined. Most are not marked by any appreciable change in grain-size texture. Evidence exists for substantial penecontemporaneous or post-depositional sediment disruption. Soft intraclasts up to 7 cm long and wispy trains of light- or dark-toned diatom ooze are commonly included in ooze of another tone (and thus volcanic content). Some intraclasts show internal bedding in the form of sandy laminae (e.g., core photograph of 119-736A-8H-3, 110–120 cm; 52 mbsf), and such laminae may be inclined, bowed, and disrupted. Rare intraclasts of volcanic, sandy, laminated foraminiferal diatom ooze are also seen (e.g., Section 119-736A-4H-1, 74 cm; 30.2 mbsf).

Bioturbation structures are rarely seen and difficult to identify, apart from wispy segregates in the disturbed, impure, diatom oozes. The sole macroscopic benthic faunal remains detected were a scaphopod shell at 50 cm in Section 119-736A-2H-3 (12.5 mbsf) and shell fragments in Section 119-736A-14H-2 (89 mbsf).

Nonsorted units of mixed gravel, sand, and diatom ooze attain thicknesses of 40–60 cm (Cores 119-736A-3H to 118-736A-5H, 119-736A-7H to 119-736A-16H, and 119-736B-1H to 119-637B-3H; 18.5–108 mbsf). Typically they have colors from black to very dark olive gray (5Y 2.3/2 to 5Y 3/1). The coarsest components consist of subangular to subrounded basalt and pumice at granule size (usually 2–8 mm), whereas sand components consist of glass, pumice, feldspar, and basaltic lithic fragments. The estimated percentages of gravel plus sand in such units is up to 20%. Rare clasts of altered volcanics (up to 15 mm in size) and reddish (?)sandstone have been noted. Several examples show sharp upper and lower bedding contacts and coarse-tail grading. In one instance (Section 119-736A-7H-3, 75 cm; 47 mbsf), volcanic-derived granules are in the lower part of a 56-cm-thick unit that has crude grading at its base. In Section 119-736A-10H-5 (64 mbsf) 10–20-cm granules and a 2-cm basalt clast have accumulated at the base of a graded unit. Intraclasts of finer textured impure ooze are also commonly incorporated (e.g., at 60 cm in Section 119-736A-12H-3).

Pebbles and granules of basalt and pumice occur as isolated clasts (lonestones) in most of the color variations of the diatom ooze. The largest appears to reach a size of 4.5 cm (Section 119-736A-4H-1, 80 cm; 29 mbsf), but most are <2 cm. Although it is conceivable that some were incorporated in the soft sediment during drilling, many are obviously in undisturbed positions. A few of the pebbles (e.g., Section 119-736A-1H-4, 136–142 cm; 5.9 mbsf) show faceting, striations, or bullet-nose shapes. All such pebbles are of basalt or pumice, and together they amount to <1% of the core's split surface.

Well-sorted sediments are volumetrically insignificant in the *in-situ* core recovery. Where present, they are in the form of tuff layers (the highly disturbed volcanic gravels are described elsewhere in this section). Olive gray (5Y 3/2) to black (5Y 2.5/1) volcanic ash and lapilli tuffs are present in beds only a few centimeters thick in Sections 119-736A-3H-1, 119-736A-3H-2, 119-736A-6H-2, 119-736A-8H-2, and 119-736B-3H. They seem to be restricted to stratigraphic levels at approximately 18–20, 40, and 50 mbsf. The sand/gravel components are up to 7 mm in size; consist of pumice, glass, feldspar, and (?)quartz; and range from very well sorted to poorly sorted. Significantly, no diatom ooze is incorporated as matrix. The degree and form of internal size grading is variable, from none (e.g. Section 119-736A-3H-1, 49–56 cm) to normal and reverse grading in basalt (glass) and pumice sand, respectively. A fine example of this grading occurs at 128–134 cm in Section 119-736A-3H-1 (20 mbsf) where silt-sand vitric ash tuff fines upward from a sharp bed base and well-rounded pumice granules coarsen toward the sharp upper-bed boundary. Most pumice fragments are very well rounded. The bed boundaries are usually sharp, but not noticeably erosional.

Unit II

Diatom ooze with minor nannofossil ooze

Samples 119-736C-7R-2, 27 cm, to 119-736C-18R-4, 30 cm; depth, 257.1–366.1 mbsf.
Age: late Pliocene.

Unit II consists almost entirely of diatom ooze containing only traces (<1%) of volcaniclastic and terrigenous material, but with an environmentally significant 7-cm-thick nannofossil ooze at 61–68 cm in Section 119-736C-7R-2.

The diatom ooze is olive (5Y 4/3 and 5Y 4.4) to olive gray (5Y 5/4 and 5Y 5/3) and consists of 80% silt-size and 20% clay-size particles, with a mean size of 7 μm. Smear slides show a minor content of feldspathic and quartz silt, ash fragments, and glass. The nature of this siliciclastic component is quite different from that in the Unit I oozes, principally in the lack of pumice and basalt fragments and in the presence of feldspars and glass. At about 293 mbsf the unit contains traces of authigenic dolomite (Section 119-736C-10R-7, 30–60 cm). The diatom ooze is homogeneous, with no sedimentary structures in evidence. A soupy structure in parts may be due to the drilling disturbance of sediment with a high water content. Small pebbles, amounting to <1% of the core, are dispersed throughout; the largest is ~2 cm in diameter. They are mainly subangular to subrounded and are commonly faceted with some striations.

The nannofossil ooze is pale olive (5Y 6/2), lacks clastic components, and is free of diatoms. Grain-size studies reveal 2% sand, 76% silt, 22% clay, and a 9.6-μm mean size. No internal structures are apparent, but the upper and lower boundaries are abrupt.

Interpretation of Depositional Environment

The sedimentary sequence at Site 736 is dominated by two distinct components: a biogenic component characterized by siliceous diatom oozes and a volcanogenic one consisting of a mixture of basaltic gravel and pumice, plus sand- and silt-sized volcanic glass, lithics, and minerals. The supply of volcanic detritus began in the late Pliocene, but reached a climax only late in the Quaternary.

Diatom Oozes

Throughout the time represented by the sequence, deposition of diatoms continued almost without interruption and without significant reworking or disaggregation by bottom currents. The recovered cores of pure diatom ooze almost totally lack sedimentary structures (Unit II and parts of Unit I). Accumulation was therefore well below wave base, probably in bathymetric conditions similar to those of today. Bioturbation, although evident in a few places, does not appear to have been a major process.

Tuffs

The thin, well-sorted lapilli- and ash-tuff horizons that are free of diatom ooze matrix appear to represent submarine ashfall tuffs. Grain-size sorting is an important feature that is normal with mineral and glass grains, but reversed in the case of pumice grains. Upper and lower stratal boundaries are sharp and apparently not erosional. No other form of sediment structure was detected. The absence of diatom ooze, where that lithology lies above and below, implies that emplacement was not across the seafloor (density flow), but directly through the water column.

Volcanic Detritus Incorporated in Diatom Ooze

As illustrated in Figure 5 and described in this section, the diatom oozes in Unit I contain substantial components of disseminated volcanogenic gravel, sand, silt, and clay. The volcanic content is not uniformly distributed, but is concentrated in cer-

tain strata, in sandy intraclasts of diatom ooze, in units of gravelly/sandy diatom ooze, and as isolated clasts (lonestones). The data are presently not sufficient to define the origins and modes of emplacement of the detritus, but plausible hypotheses include: (1) erosion and transport on Kerguelen and Heard islands by glacial and fluvial processes, (2) distribution over the Kerguelen Plateau by ice rafting, and (3) distribution (or redistribution) in the form of gravity flows.

The well-sorted gravels that lie at the tops of cores as (1) downhole cave-in contamination, (2) gravels that are in place but disturbed by the drilling, and (3) *in-situ* gravel deposits are particularly difficult to interpret. Frohlich (1983), Leclaire (1983), and Schlich and Leclaire (1981, 1983) documented similar gravels forming a surficial or barely buried apron over the Kerguelen Plateau near Kerguelen Island. Although the Leg 119 Shipboard Scientific Party agreed that most core top gravels were downhole contamination derived from these near-surface gravels, some sedimentologists regarded the gravels of Sections 119-736A-1H and 119-736A-7H-1 as *in situ* but drilling disturbed.

The origin of the gravel material, however, is reasonably in evidence. All lithologies can be related to the Kerguelen and Heard islands' volcanic centers and are, therefore, of local derivation. The extent of glacial processes in erosion and subsequent gravel transport and emplacement is not precisely known but is evidenced in the occurrence of striated, bullet-nosed, and distinctively faceted clasts, which imply transport at some stage at the base of a wet-based glacier. Furthermore, some lonestones that can be interpreted as ice-rafted debris occur in all color variations of diatom ooze (implying that they are independent of the volcanic sand-silt-clay supply) and are most commonly associated with high contents of this finer material. Unfortunately, a lack of fine bedding in the core prevents the recognition of true dropstone structures. Kerguelen and Heard islands are currently glaciated, and their geomorphology suggests more extensive glaciation in the past (Nougier, 1970), extending into marine environments and involving the calving of tidewater glaciers. According to this hypothesis, the gravels found at Site 736, whether at the core tops, disseminated in the impure diatom ooze, or in the form of lonestones, were emplaced as ice-rafted debris.

In many of the units of diatom ooze with disseminated gravel-sand-silt-clay volcanic material, sediment textures and structures imply some transport and emplacement by density-flow processes. We observed clear instances of sharp basal contacts with crude size grading of the gravel and coarse sand components, incorporation of soft intraclasts of volcanic-bearing ooze and relatively pure ooze, apparent post-depositional disturbance of bedding relations with irregular and locally highly inclined boundaries, and diffuse and wispy lithologic boundaries. As already noted, bioturbation was not an important process in this regard. Identification of the volcanic-bearing diatom oozes as density-flow deposits of a type described as a "disorganized turbidite" (Stow and Piper, 1984) would explain the preceding features. The physical behavior of such sediments is not well known, but it may be speculated that they represent immature states of density-current flow (before size grading) or short-lived turbidity currents. The behavior of diatom ooze in density flows is not well documented. A density-flow origin is consistent with the high observed sedimentation rates (see "Sedimentation Rates" section, this chapter) and local Quaternary seafloor gradients.

BIOSTRATIGRAPHY

An apparently biostratigraphically continuous 371-m-thick sequence of upper Pliocene to Pleistocene diatom oozes with minor volcaniclastics was recovered at shallow-water (629 m) Site 736 on the northern Kerguelen Plateau.

Recovery, lithology, biostratigraphic ages and corresponding biozones, the abundance and preservation of the various fossil groups, and some additional sedimentologic information gained from the analyses of all core-catcher samples available are summarized in Figure 6. Biostratigraphic age assignments of this neritic section are based almost exclusively on diatoms. No useful paleomagnetic data are recoverable.

Abundant, well-preserved, and highly diverse diatom assemblages dominate the biogenous components throughout the recovered interval. Radiolarians are abundant and well preserved. Low coarse-fraction percentages consist of mostly terrigenous, detrital particles, with some foraminifers and abundant large diatoms. Low-diversity subpolar planktonic foraminifers decrease in abundance below the Pliocene/Pleistocene boundary. Mostly well-preserved benthic foraminifers are rare to common throughout the recovered interval. Most core-catcher samples are barren of calcareous nannofossils. A few moderately etched, monospecific, subpolar nannofossil assemblages are present in a gravelly horizon at 60 mbsf and between 200 and 250 mbsf. Low-diversity silicoflagellate assemblages occur throughout the recovered sequence. The section is devoid of organic-walled microfossils.

Calcareous Nannofossils

Calcareous nannofossils are either absent or very rare in all core-catcher samples investigated from Site 736. Mud-line Sample 119-736A-1H, 0–2 cm, contained rare, well-preserved *Gephyrocapsa oceanica*. In the upper 250 m of the sedimentary section only moderately to strongly etched *Coccolithus pelagicus* were encountered in Samples 119-736A-9H-CC (rare), 119-736A-25X-CC (rare), 119-736A-27X-CC (few), 119-736A-29X-CC (common), 119-736A-30H-CC (rare), 119-736C-4R-CC (rare), 119-736C-5R-CC (few), 119-736C-6R-CC (rare), and 119-736C-7R-CC (few). Sample 119-736C-7R-2, 66 cm, from a thin layer (about 5 cm thick) of calcareous nannofossil–diatom ooze at 257 mbsf contained a well-preserved monospecific assemblage of *Reticulofenestra perplexa* (= *Dictyococites antarcticus* Haq). Sample 119-736C-8R-CC contained strongly etched *C. pelagicus* (few) and *Gephyrocapsa* sp. (rare), and a few, moderately well-preserved *Reticulofenestra perplexa* were found in Sample 119-736C-9R-CC.

These nannofossils are of limited biostratigraphic value. The upper 250 m section can be assigned to the Pliocene through Pleistocene, and the interval from 250 to 280 mbsf is probably Pliocene in age.

The absence or scarcity of calcareous nannofossils in the upper Neogene diatom oozes on Kerguelen Plateau seems to be due to lack of supply instead of preservation.

Foraminifers

The 371 m of lower Pliocene through Quaternary sediments recovered at Site 736 is carbonate poor, mainly consisting of siliceous oozes with interspersed volcanogenic clasts, basaltic gravels, and glacial dropstones. Foraminifers were studied from the mud-line sample (0–2 cm) and all core-catcher samples from Holes 736A, 736B, and 736C. The occurrence of a few stained specimens (Rose Bengal) in the mud-line sample indicates only a small loss of the surface layer through the drilling operation. The relative abundance of species from the >150-μm fraction was estimated for each sample (see "Explanatory Notes" chapter). The abundance of foraminifers varies downcore and shows a changing planktonic/benthic ratio. Below a depth of 313 mbsf (Core 119-736C-12R) no foraminifers were found. The recovered assemblages show typical features of the Antarctic region: low diversity and lacking age-diagnostic species. Test preservation is good down to Core 119-736A-17X (118 mbsf), where calcite encrustation becomes apparent on some planktonic foraminifers. The benthic specimens are generally well preserved throughout the range of their occurrence.

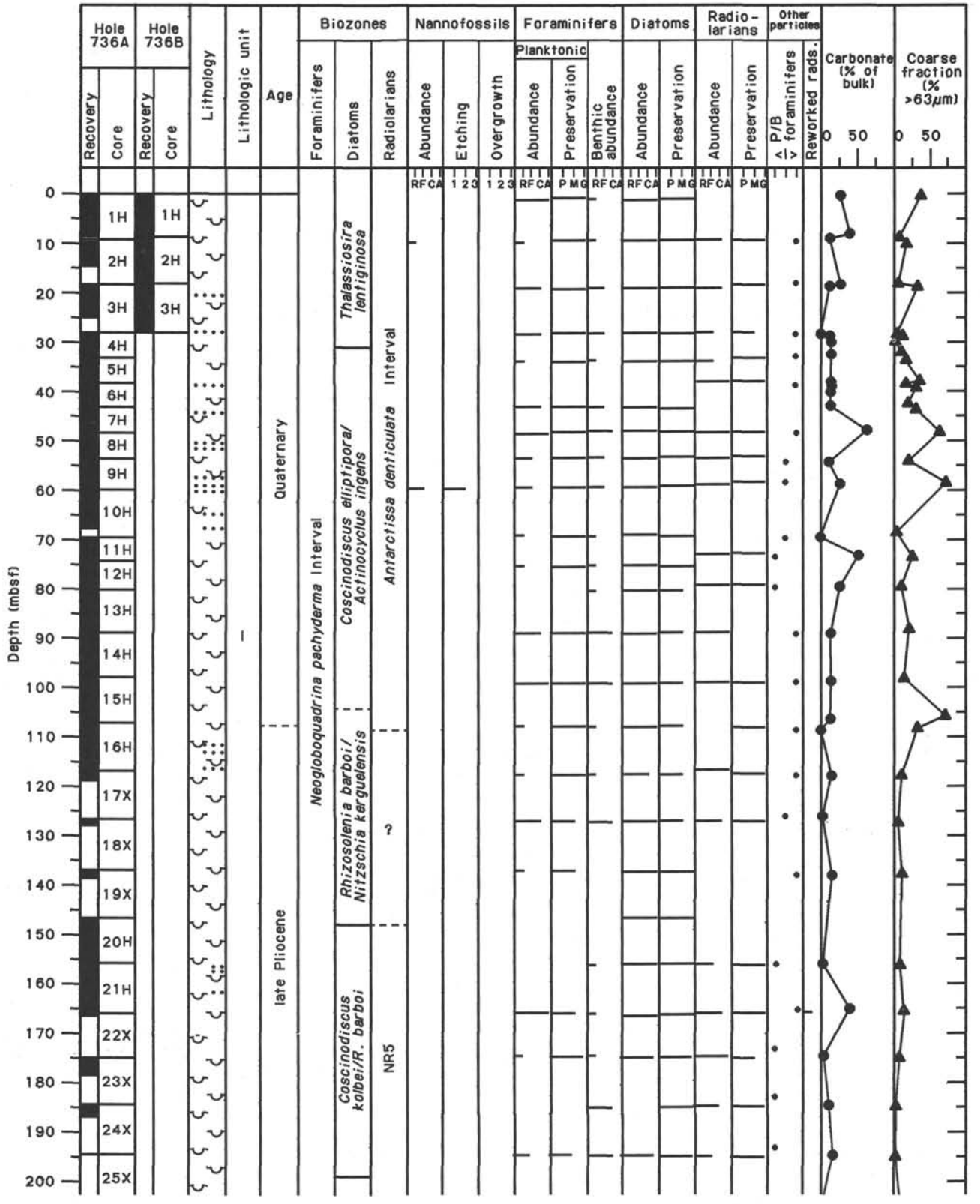

Figure 6. Biostratigraphic summary, Site 736.

Planktonic Foraminifers

Most foraminifer assemblages above Core 119-736A-25X (195 mbsf) are dominated by sinistrally coiled specimens of *Neogloboquadrina pachyderma*. Planktonic foraminifers below this interval occur in decreasing abundance and are absent below Core 119-736C-8R (255 mbsf). Other planktonic species found at this site include *Globigerina bulloides*, which occurs sporadically and

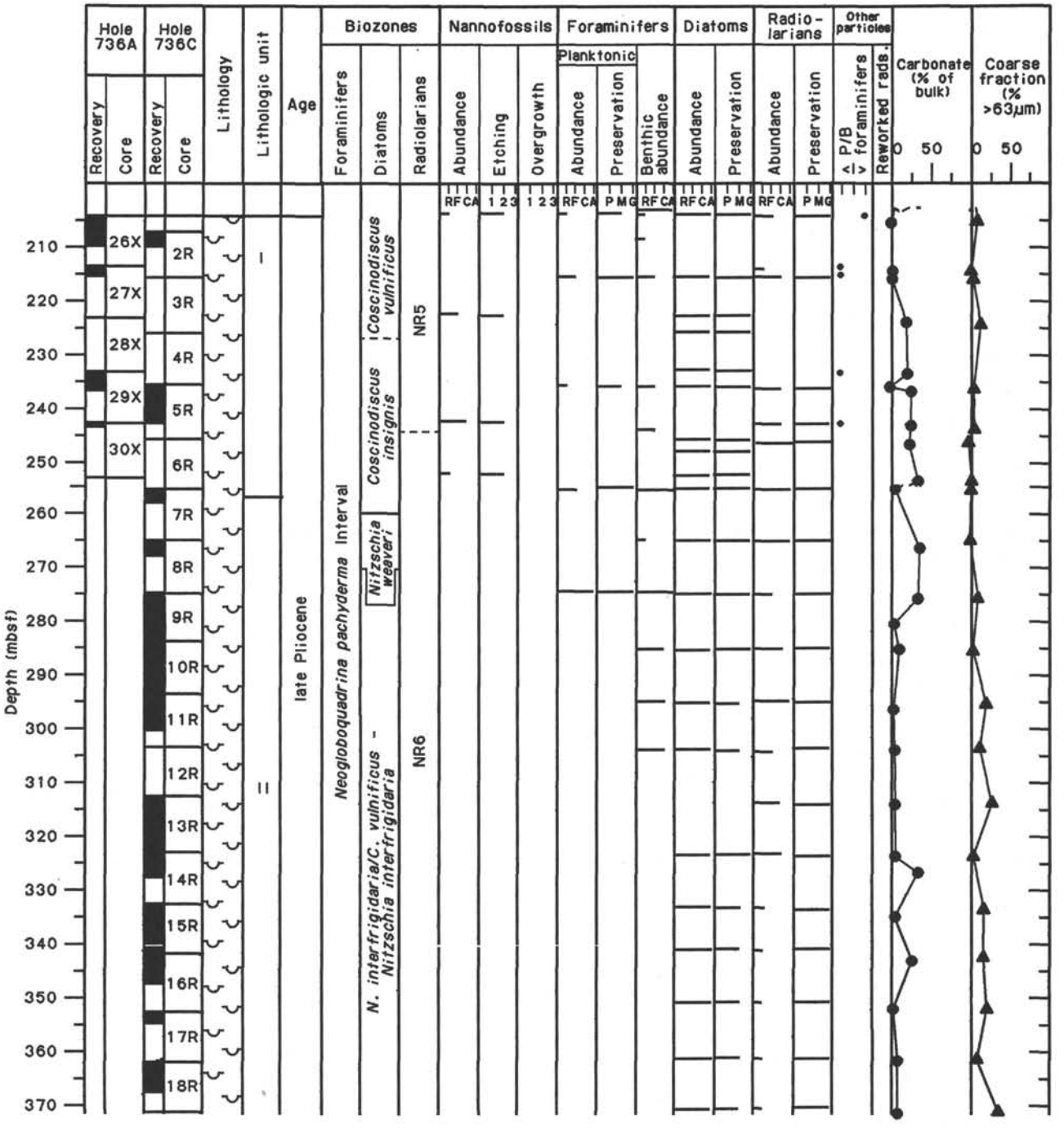

Figure 6 (continued).

in low abundance to a depth of 223 mbsf, *Globorotalia crassaformis*, found in low to moderate abundance in Cores 119-736A-9H, 119-637A-21H, 119-736A-22X, and 119-736C-6R, and several specimens of *Globigerinoides quadrilobatus*, found in Cores 119-736A-21H, 119-736A-25X, and 119-736C-6R. Of these species, *G. crassaformis* provides the best age control, as it has a reported range of late early Pliocene (upper Zone N19) to Holocene (Kennett and Srinivasan, 1983). The other taxa have been reported from late Miocene age or older sediments.

Benthic Foraminifers

Benthic foraminifers are dominated by calcareous species throughout the entire sequence. The assemblage is characterized by a relatively low diversity and only a few dominant species. The abundant taxa include *Cassidulina oblonga, Bulimina aculeata, Sphaeroidina bulloides, Melonis barleanum, Angulogerina earlandi, Pullenia bulloides*, and *Globobulimina pacifica*. The fluctuation of these dominant species marks the changes in

the assemblage through time that may indicate changes in bottom-water conditions.

The Quaternary and upper Pliocene interval above Sample 119-736C-9R-CC is characterized by an alternating dominance of *C. oblonga, B. aculeata, A. earlandi, S. bulloides*, and *M. barleanum*. Accompanying species with a less dominant occurrence include *Angulogerina angulosa, Cassidulina laevigata, Pullenia subcarinata, Stainforthia complanata, P. bulloides, Bolivina earlandi, Globocassidulina subglobosa*, and several rare species.

Within the interval from Cores 119-736C-9R through 119-736C-11R, the assemblage changes to a fauna dominated by *G. pacifica* and *Buliminella elongata*. Both species are absent in the sequence above Sample 119-736C-9R-CC. Benthic foraminifers are rare or completely absent from the siliceous ooze sequence that spans the Quaternary/Pliocene boundary.

Agglutinated species are represented only in the mud-line sample by single specimens of *Recurvoides scitulus, Reticulophragmium trullissatum, Trochammina globigeriniformis*, and *Textularia earlandi. Martinotiella antarctica* is preserved in the fossil record but was rarely found downcore. This species uses siliceous cement and is reported to occur predominantly in diatomaceous sediments (Echols, 1971). *M. antarctica* is also found in downcore sediments at Site 695 in the Weddell Sea (Shipboard Scientific Party, 1988). The sparse agglutinated fauna at this site contrasts with a study of surface samples on the western slope of the Kerguelen Ridge, west of Head Island, where an agglutinated component of 21% (at 790 m depth) was found (Lindenberg and Auras, 1984). The calcareous component in the surface study yields a high abundance of *A. earlandi* and *B. aculeata*, which compares with the Holocene fauna of Site 736.

Interpretation of changes in the benthic foraminifer assemblage will depend on results from oxygen and carbon isotopic analyses of the planktonic species *Neogloboquadrina pachyderma*, as benthic taxa are too sparse. These results may define the effect of the lateral shifts of the Polar Front on the deep-water environment.

Diatoms

Diatoms are abundant in all core-catcher samples examined from Site 736. Preservation is generally good with sporadic samples exhibiting moderate preservation. The lowermost samples (119-736C-17X-CC and 119-736C-18X-CC) have poor preservation. The majority of the species present are characteristic of the Southern Ocean; however, some species present are more typical of the middle latitudes.

Stratigraphic indicators are common and allow recognition of the Southern Ocean diatom zonation of Ciesielski (1983). Zonal boundaries defined by Ciesielski (1983) on the last occurrence of *Nitzschia weaveri, Nitzschia interfrigidaria*, and *Cosmiodiscus insignis* are recognized in this study at the last common occurrence rather than at the last occurrence of these species.

The stratigraphic sequence recovered from Site 736 is Pliocene and Quaternary in age and can be divided into nine diatom zones. The last occurrence of *Actinocyclus ingens* in Sample 119-736A-4H-CC and the absence of this species in Sample 119-736B-3H-CC allows placement of Cores 119-736A-1H through 119-736A-3H and 119-736B-1H through 119-736B-3H into the *Thalassiosira lentigenosa* Zone (previously the *Coscinodiscus lentiginosus* Zone) of Ciesielski (1983). Thus, these intervals have an estimated age younger than 0.62 Ma. The assemblage present in these intervals is dominated by *Nitzschia kerguelensis* and *Eucampia antarctica*.

The last occurrence of *Rhizosolenia barboi* in Sample 119-736A-15H-CC suggests that the interval from 119-736A-4H-CC through 119-736A-14H-CC is equivalent to the *Coscinodiscus elliptopora/Actinocyclus ingens* Zone of Ciesielski (1983). However, placement of this zonal boundary is tentative because *R. barboi* has a sporadic occurrence in the uppermost part of its stratigraphic range. Supporting the zonal assignment is the occurrence of *Coscinodiscus elliptopora* in Cores 119-736A-8H through 119-736A-16H. The last occurrence of *Coscinodiscus kolbei* between Cores 119-736A-18X and 119-736A-20H defines the base of the *C. elliptopora/A. ingens* Zone. This zonal interval is dominated by *N. kerguelensis, T. lentigenosa*, and *A. ingens*.

Cores 119-736A-15H through 119-736A-18X (no core was recovered from 119-736A-19X) are assigned to the *Rhizosolenia barboi/Nitzschia kerguelensis* Zone, which is defined as the interval from the last occurrence of *C. kolbei* to the last occurrence of *R. barboi*. This interval is characterized by *N. kerguelensis, R. barboi, A. ingens, T. lentigenosa, Thalassiosira gracilis*, and *Thalassionema* sp.

The last occurrence of *C. kolbei* in Sample 119-736A-20H-CC and the last occurrence of *Coscinodiscus vulnificus* in Sample 119-736A-25X-CC allow Cores 119-736A-20H through 119-736A-24X to be placed into the *Coscinodiscus kolbei/Rhizosolenia barboi* Zone. *A. ingens, C. kolbei, Nitzschia angulata, N. kerguelensis, Thalassionema* sp., and *T. lentigenosa* dominate the diatom assemblage in this interval.

The last occurrence of *C. vulnificus* in Sample 119-736A-25X-CC, the last common occurrence of *C. insignis* between Samples 119-736A-27X and 119-736A-29X-CC, and the last common occurrence of *N. weaveri* in Sample 119-736C-7R-CC indicate that Cores 119-736A-25X through 119-736A-30X and 119-736C-2R through 119-736C-6R are equivalent to the *Coscinodiscus vulnificus* and *Cosmiodiscus insignis* Zones. The boundary between these zones is tentatively placed between Cores 119-736A-27X and 119-736A-29X and between Cores 119-736C-6R and 119-736C-7R, respectively. *C. insignis, N. angulata*, and *Thalassionema* sp. typify this interval.

Core 119-736C-8R is assigned to the *Nitzschia weaveri* Zone based on the last common occurrence of *N. weaveri* in Sample 119-736C-7R-CC and the last common occurrence of *N. interfrigidiaria* in Sample 119-736C-8R-CC. *Actinocyclus karsteni, N. weaveri, C. kolbei, C. insignis, Paralia sulcata*, and *Thalassionema* sp. characterize the assemblage in this sample.

The sporadic occurrence of *C. vulnificus* in the lower part of its stratigraphic range requires that the *N. interfrigidiaria/C. vulnificus* Zone be combined with the *Nitzschia interfrigidaria* Zone. The base of this zonal interval is defined as the first occurrence of *N. weaveri*. Cores 119-736C-9R through 119-736C-18R are assigned to this combined zone based on the occurrence of *N. interfrigidiaria, Thalassiosira lentigenosa* var. *obovatus, N. angulata, N. weaveri, T. gracilis*, and rare specimens of *Nitzschia praeinterfrigidaria*. Based on the diatom stratigraphy, the base of Hole 736C is younger than 3.8 Ma.

Radiolarians

Holes 736A and 736B

Radiolarians are generally common and well preserved throughout the cores of Holes 736A and 736B. They are few or rare in Cores 119-736A-1H, 119-736A-3H, 119-736A-4H, 119-736A-20H, and 119-736A-23X through 119-736A-26X. No barren samples were found. Sediments range in age from Quaternary to late early Pliocene.

Quaternary

Compared to the pelagic faunas described in subantarctic sediments (Chen, 1975; Weaver, 1983), the Pleistocene radiolarian assemblage from Holes 736A and 736B contains very few species (15 to 20). The absence of many stratigraphic markers such as *Stylatractus universus, Saturnalis circularis,* and *Phormostichoartus pitomorphus*, which appear to be deep-living pelagic radiolarian species, reflects eutrophic conditions. This association of radiolarians and the great abundance of diatoms is indicative of local upwelling conditions. The subantarctic zonation cannot be used, and Zones NR1 through NR4 are described as the "*Antarctissa denticulata* Interval." Sample 119-736A-1H-CC contains a typical upper Quaternary Antarctic radiolarian assemblage that can be assigned to the NR1 Zone by comparison with previously studied Kerguelen Plateau material (Caulet, 1986). Common species include *Antarctissa denticulata, Spongotrochus glacialis, Theocalyptra bicornis, Theocalyptra davisiana, Saccospyris antarctica*, and *Triceraspyris antarctica*. Sample 119-736A-7H-CC contains *Pterocanium trilobum* and falls within the upper part of the NR3-4 Zone (= *S. universus* Zone; Weaver, 1983). The last appearance of *Antarctissa ewingi* occurs in Sample 119-736A-8H-1, 53–55 cm.

Pliocene

The last occurrence of *Clathrocyclas bicornis* in Sample 119-736A-20H-1, 63–65 cm, places this sample in Zone NR5. Radiolarians are rare and apparently winnowed in Sample 119-736A-20H-CC. Sample 119-736A-21H-CC contains a typical late Pliocene age fauna with *C. bicornis, Antarctissa ewingi, T. davisiana*, and very few *A. denticulata*. This assemblage is found in Samples 119-736A-21H-CC through 119-736A-27X-CC, and the interval falls within the upper Pliocene Zone NR5. First occurrence of *Lithelius nautiloides* is observed in Sample 119-736A-20H-CC. The first occurrence of *T. davisiana* is in Sample 119-736A-23X-1, 35–37 cm. This datum occurs within the upper Gauss Chronozone and has an estimated age between 2.6 and 2.8 Ma (Weaver, 1983).

Samples 119-736A-29X-CC and 119-736A-30X-CC are upper lower Pliocene. The last occurrences of *Desmospyris spongiosa* and *Pseudocubus vema* in Sample 119-736A-29X-1, 53–55 cm, mark the top of the NR6 Zone. The radiolarian assemblage is well preserved, but neither warm water- nor deep-water species are reported.

Hole 736C

Radiolarians are well preserved in all cores from Hole 736C. Sample 119-736C-2R-CC contains a Quaternary assemblage that can be assigned to the "*A. denticulata* Interval." Samples 119-736C-4R-CC through 119-736C-18R-CC are upper lower Pliocene, and can be assigned to the NR6 Zone. The last occurrence of *Theocorys redondoensis* occurs in Sample 119-736C-11R-CC. This species is common throughout the hole.

Palynology

Twenty-six core-catcher samples from Hole 736A (Cores 119-736A-1H through 119-736A-16H, 119-736A-18X, 119-736A-20H through 119-736A-26X, 119-736A-28X, and 119-736A-30X) were processed for palynomorphs. Only one species of dinoflagellate cyst, *Tectacodinium pellitum*, was recorded. This form, which occurred only in very low abundance in five core-catcher samples (Cores 119-736A-2H through 119-736A-4H, 119-736A-6H, and 119-736A-14H) has a long stratigraphic range (Paleocene-Pleistocene). Its first appearance downhole in the second core of Hole 736A is probably consistent with a Pleistocene age for this part of the succession.

Other Organisms

An arm of a live ophiuroid (R. Hessler, pers. comm., 1988) was found in Sample 119-736A-1H-1, 80 cm. Sporadic mollusk shells (mostly scaphopods) were preserved in several cores.

PALEOMAGNETICS

Three holes were drilled at Site 736. The sediments from Holes 736A and 736B were collected using the APC coupled to the Multishot core-orientation tool. Thus, Cores 119-736A-5H through 119-736A-21H and 119-736B-1H through 119-736B-3H were oriented and are potentially important for paleomagnetic stratigraphy. The Multishot orientations as well as the magnetic declination correction (−52°W) were used to reorient sample declinations into the corrected Earth's magnetic field coordinates. Results for Hole 736A are shown in Figure 7; however, because of the unstable natural remanent magnetization (NRM), the results cannot be used to define the record of the polarity history here. Future shorebased demagnetization experiments are necessary.

Because of the lack of liquid helium aboard ship at the time of drilling, the cryogenic magnetometer could not be used to measure whole cores. Instead, discrete paleomagnetic samples were collected and measured on the Molspin spinner magnetometer. We collected 287 samples from Hole 736A, 35 oriented samples from Hole 736B, and 31 samples from Hole 736C (rotary coring). In washing down to the desired drilling depths, however, the muds from Hole 736C were liquified, causing deformation of the samples. Thus, only limited samples were collected from this hole.

The NRM directions and intensities from these samples are plotted stratigraphically in Figures 7 through 9. All of the samples collected from Site 736 are green diatomaceous oozes, with magnetic intensities that are quite low (90 to 0.05 mA/m). The low magnetic intensities reflect the reduced magnetic minerals in the sediments. The results of the paleomagnetic measurements are extremely scattered; therefore, polarity designations cannot reliably be made on the basis of these data.

Limited shipboard three-axis alternating field (AF) demagnetization was carried out on a pilot set of representative samples from the cores. A broad spectrum of stability behavior can be observed in the demagnetization studies. Only one sample studied displayed moderate magnetic stability (see Fig. 10). The results of the demagnetization of Sample 119-736A-9H-2, 38–40 cm, show that after demagnetization at 2 mT, the sample direction stabilized with a reversed direction and moderate paleolatitude (positive inclination) at demagnetization levels between 4 and 20 mT. An orthogonal plot of the pilot sample data shows that a strong secondary component of magnetization affects most of the samples. Usually much of this component can be removed during the first demagnetization step. Sample 119-736A-6H-2, 85–87 cm, lost 80% of the normalized intensity after a single demagnetization step at 2 mT. Other samples (e.g., Samples 119-736A-6H-3, 110–112 cm, and 119-736A-9H-2, 69–71 cm) display higher magnetic coercivities but fail to stabilize in direction with demagnetization in fields up to 30 mT.

The results of the initial shipboard magnetic measurements of the sediments from Site 736 indicate that the sediments from Holes 736A, 736B, and 736C are characterized by magnetic carriers that are not stably magnetized. The sediments are weakly magnetized, making initial measurements difficult. Further detailed demagnetization in a low-ambient magnetic field environment may succeed in identifying some samples with stable magnetization that could be used to reliably determine magnetic polarity. However, the initial investigations completed in the locally strong magnetic fields of the drillship were not successful in

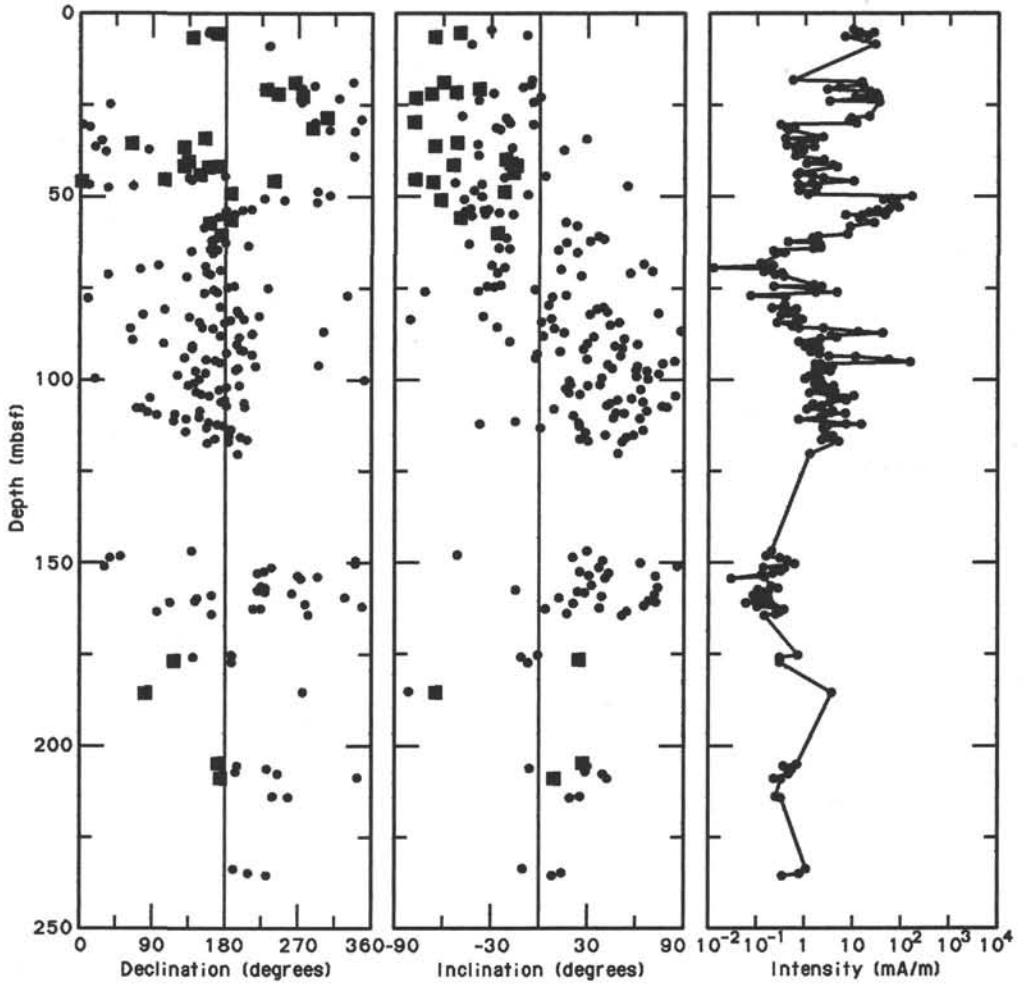

Figure 7. Stratigraphic plot of declination, inclination, and intensity for samples from Hole 736A. NRM values are plotted as circles, and data for samples demagnetized using an alternating field (peak value 30 mT) are plotted as squares.

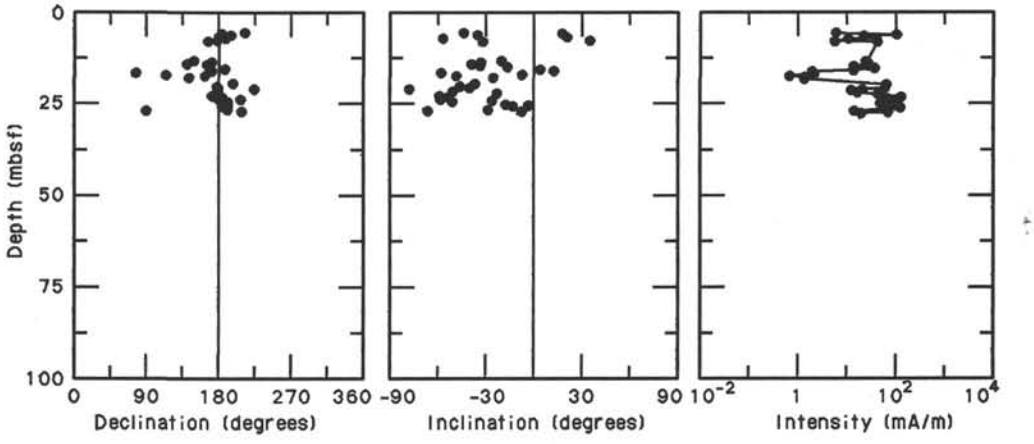

Figure 8. Stratigraphic plot of declination, inclination, and intensity for samples from Hole 736B.

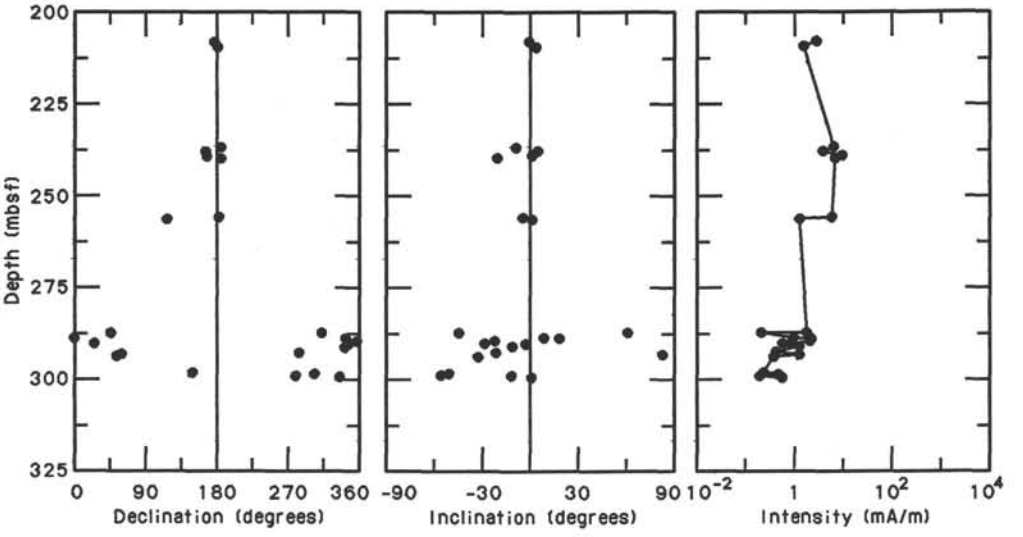

Figure 9. Stratigraphic plot of declination, inclination, and intensity for samples from Hole 736C.

identifying the stable components of magnetization or the magnetic polarity sequence.

Magnetic Susceptibility

All recovered sections of Hole 736A were measured using the Bartington Instruments M.S.1 susceptibility meter at the 0.1 sensitivity and low-frequency (0.47-kHz) settings (Fig. 11). The cores were measured at 20-cm intervals. The volume susceptibility varies between 0.2×10^{-6} and 889.3×10^{-6} cgs units. The NRM intensity and susceptibility values in Figure 11 have a strong correlation. The frequent spikes in the susceptibility measurements are probably the result of rust within the cores.

SEDIMENTATION RATES

Biostratigraphic control at Site 736 relies on both diatom and radiolarian stratigraphies ("Biostratigraphy" section, this chapter). The stratigraphic constraints used to construct the sedimentation-accumulation rate curve are summarized in Table 4. With the exception of the first occurrence of the radiolarian *Cycladophora davisiana*, all of the events fall on a dog-legged linear plot. Because the first occurrence of *C. davisiana* suggests an age older than that suggested by the other events, we assume that the range of *C. davisiana* is ecologically controlled at this site.

Two main segments characterize the sediment-accumulation rate curve shown in Figure 12.

1. Between 0 and about 80 mbsf, the mean sedimentation rate is estimated to be 54 m/m.y. This rate is based on the last occurrence of the diatom *Actinocyclus ingens*, assuming a continuous stratigraphic sequence and an age of 0 Ma for the topmost sediment.
2. Between about 80 and 370 mbsf, the numerous diatom events allow the calculation of a mean sedimentation rate of about 140 m/m.y. The change in the sedimentation rate is placed at 80 mbsf; however, such a placement is arbitrary because it is based on one biostratigraphic event and assumes stratigraphic continuity. The base of the hole has an extrapolated age of 3.5 Ma (latest early Pliocene).

INORGANIC GEOCHEMISTRY

A total of 14 whole-round 5-cm-long minicores were obtained from Holes 736A and 736C for the purpose of interstitial-water chemical analyses (see Table 5). All of the sediment intervals sampled for interstitial waters are composed of diatomaceous ooze with varying amounts of volcanogenic material (see "Lithostratigraphy and Sedimentology" section, this chapter). Most of the minicores contained $<5\%$ calcium carbonate and $<1\%$ organic carbon. The porosities and water contents of the samples are high, ranging from around 50% to 90% and from 40% to 80%, respectively (see "Physical Properties" section, this chapter). The four interstitial-water samples taken from Hole 736C are from RCB cores, and as these sediments are unconsolidated, RCB coring resulted in a great deal of sediment disturbance; the interstitial waters from Hole 736C are undoubtedly mixtures of drilling fluids and primary pore fluids. These samples are included in the Site 736 data set and constitute the four deepest data points in the following figures. These data will not be considered in this report.

The high sedimentation rates, shallow water depth, and high content of biogenic sediment encountered at Site 736 suggest that these sediments might be good high-latitude, open-ocean analogs of some hemipelagic sequences deposited under highly productive surface waters along continental margins (e.g., Peru margin, Southern California borderland, Gulf of California, etc.). The interstitial-water chemistry at Site 736 is, however, quite different than that encountered in other areas of high biological productivity (Gieskes et al., 1982). No major redox boundaries were identified from the interstitial-water chemical analyses at Site 736. Little, if any, variation as a function of depth below the seafloor occurs in salinity, chloride, calcium, magnesium, pH, alkalinity, and sulfate in Hole 736A. There is no evidence for significant levels of sulfate reduction within the sediment column at Site 736 based on the interstitial-water data from Hole 736A. The maintenance of sulfate concentrations near standard seawater values (28.9 mmol/L for the IAPSO standard) to 200 mbsf requires the maintenance or continual replenishment of dissolved oxygen concentrations during sediment burial.

Phosphate, silica, and ammonium are the only chemical species that show significant variations in their interstitial-water concentrations as a function of depth in Hole 736A. Dissolved phosphate concentrations are about five times greater than those in average seawater near the sediment/water interface and decrease with depth whereas ammonium concentrations increase as a function of depth. These trends are indicative of microbial

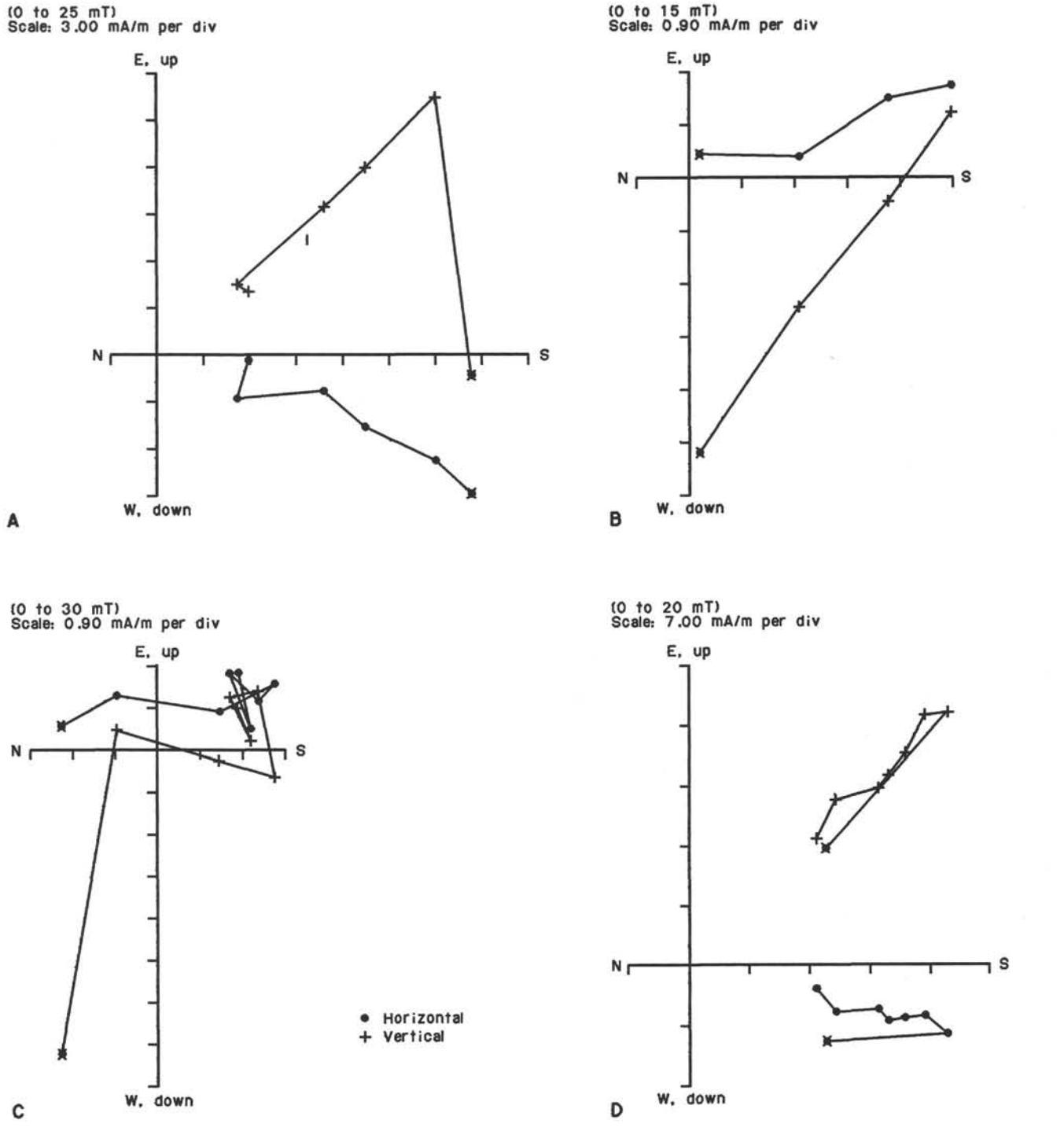

Figure 10. Orthogonal plots of sample demagnetization vectors for pilot samples from Hole 736A. **A.** Sample 119-736A-9H-2, 69–71 cm. **B.** Sample 119-736A-6H-3, 110–112 cm. **C.** Sample 119-736A-6H-2, 85–87 cm. **D.** Sample 119-736A-9H-2, 38–40 cm.

degradation of organic matter within the sediment column, but not at sufficiently high levels to exhaust the dissolved oxygen in the interstitial waters. The highest phosphate and ammonium concentrations measured at Site 736 are quite low in comparison to those encountered in sediments deposited below highly productive surface waters (e.g., Peru margin; Suess, von Huene, et al., 1988). Much of the organic matter associated with these biogenic sediments may have been lost, or rendered unreactable, prior to deposition at Site 736.

Methods

All sediment minicores were squeezed for interstitial waters immediately after retrieval from the seafloor. All of the analyses were completed within five days of coring. Each of the samples was analyzed for salinity, chloride, calcium, magnesium, sulfate, silica, pH, alkalinity, sulfate, ammonium, and phosphate. Details of the analytical methods used can be found in the "Explanatory Notes" chapter.

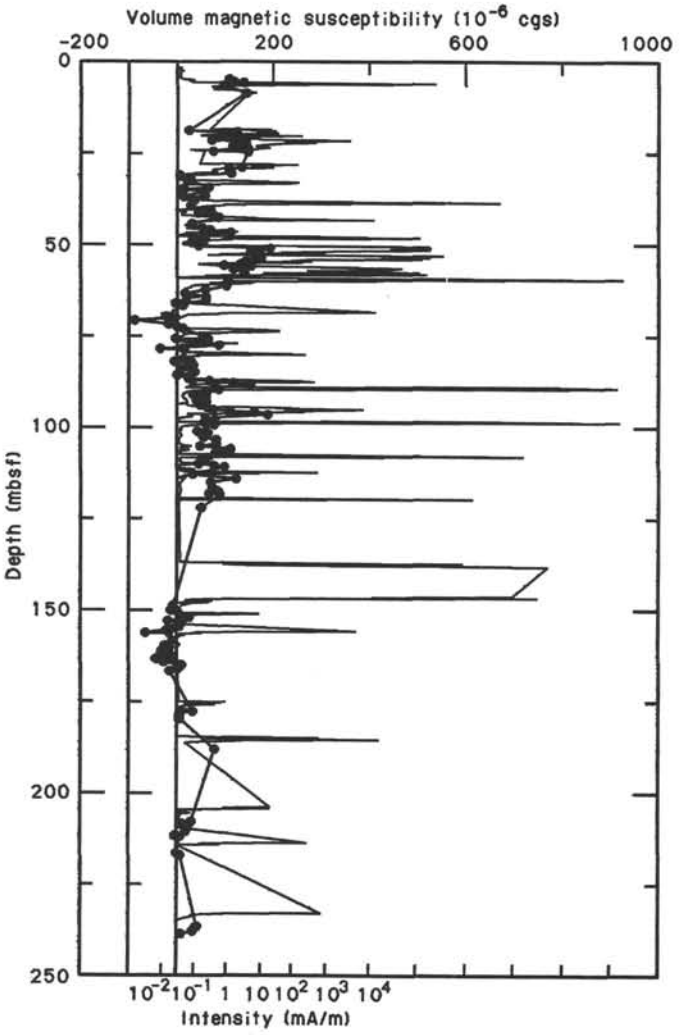

Figure 11. Stratigraphic plot of magnetic susceptibility (plotted as line trend) with NRM discrete sample intensity measurements (solid circles) superimposed. There is good agreement between susceptibility and magnetic intensity.

Table 4. Biostratigraphic markers and their estimated ages, Site 736.

Event[a]	Depth (mbsf)	Age (Ma)
L *Actinocyclus ingens*	28.0–33.0	0.62
L *Rhizosolenia barboi*	98.5–108.0	1.58
L *Coscinodiscus kolbei*	136.8–155.9	1.89
T *Clathrocyclas bicornis*	127.1–147.0	1.6–1.8
L *Coscinodiscus vulnificus*	194.3–203.9	2.22
LC *Cosmiodiscus insignis*	232.9–242.6	2.49
LC *Nitzschia weaveri*	255.9–264.7	2.64
LC *Nitzschia interfrigidaria*	264.7–274.4	2.80
F *Cycladophora davisiana*	175.0–194.3	2.6–2.8
F *N. weaveri*	>371.0	<3.88
F *Pseudocubus vema*	>371.0	<3.9

[a] L = last occurrence; LC = last common occurrence; F = first occurrence.

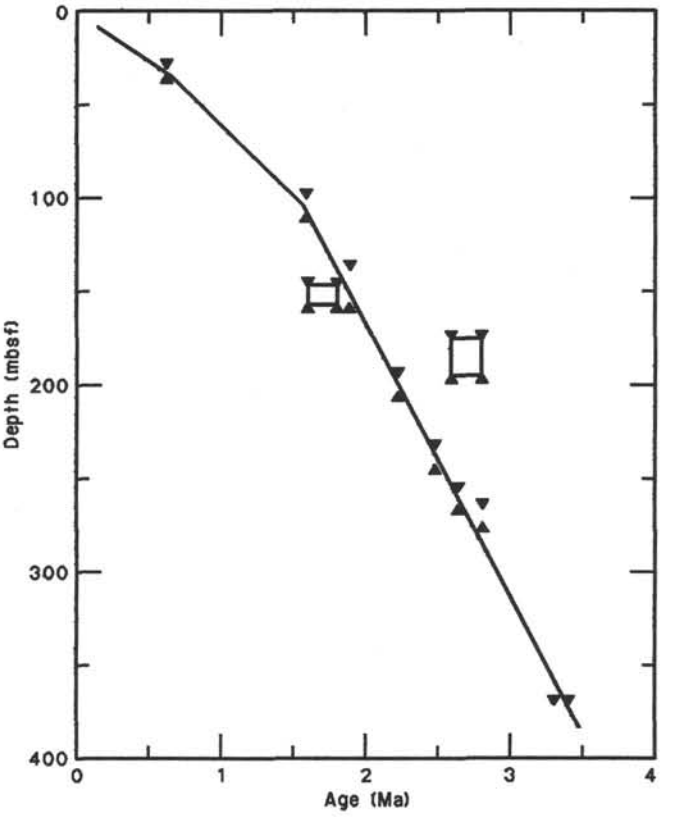

Figure 12. Sediment-accumulation rate curve for Site 736. Refer to Table 4 for events.

Results

Salinity and Chloride

Salinity and chloride concentrations remain near standard seawater levels (IAPSO chlorinity is 559 mmol/L) and show little variation throughout Hole 736A (0 to 252.3 mbsf) (Fig. 13).

Calcium and Magnesium

Magnesium and calcium concentrations do not change significantly as a function of depth in Hole 736A (Fig. 13). The concentrations of calcium and magnesium in all of the Site 736 interstitial-water samples are close to standard seawater values (10.55 and 54.0 mmol/L, respectively, in IAPSO). The low magnesium to calcium ratios (Fig. 13) in all of the samples rule out the possibility of significant authigenic dolomite formation.

Silica

The sediments cored in Hole 736A are rich in biogenic silica (opal-A), resulting in high dissolved silica concentrations in all of the analyzed interstitial-water samples (Fig. 13). Average seawater (about 89 μmol/L silicic acid; Stumm and Morgan, 1970) is greatly undersaturated with respect to amorphous silica (Krauskopf, 1956). Dissolved silica concentrations in Hole 736A increase with depth to 1130 μmol/L at 234.35 mbsf. Thus, significant silica dissolution is occurring in Hole 736A.

pH, Alkalinity, and Sulfate

After increases in the first 23 m of the sediment section, pH, alkalinity, and sulfate all show little variation with depth to the bottom of Hole 736A (Fig. 13). The increase in sulfate concentration downward from Samples 119-736A-1H-4, 145–150 cm, to 119-736A-3H-3, 145–150 cm, is suspect because it is difficult

Table 5. Interstitial-water geochemical data for Site 736.

Core, section, interval (cm)	Depth (mbsf)	Salinity (g/kg)	Chloride (mmol/L)	Calcium (mmol/L)	Magnesium (mmol/L)	Mg^{2+}/Ca^{2+}	Silica (μmol/L)	pH	Alkalinity (mmol/L)	Sulfate (mmol/L)	Ammonium (mmol/L)	Phosphate (μmol/L)
119-736A-												
1H-4, 145–150	5.95	35	556	10.08	51.6	5.12	725	7.3	3.32	17.54	0.14	16.69
3H-3, 145–150	22.95	35	557	10.24	51.7	5.05	767	7.7	5.00	24.76	0.28	13.08
6H-2, 145–150	40.95	35	562	10.46	54.0	5.16	922	7.8	4.90	24.45	0.25	10.12
9H-2, 145–150	55.95	35	559	10.35	53.1	5.13	836	7.6	4.58	25.66	0.25	6.38
13H-4, 145–150	85.45	36	556	10.55	54.6	5.18	862	7.5	4.20	22.95	0.31	5.61
16H-4, 145–150	113.95	36	560	10.12	54.0	5.33	984	7.6	4.17	25.36	0.33	4.32
20H-4, 145–150	152.35	36	559	9.98	53.5	5.36	999	7.7	4.49	16.03	0.38	3.80
23X-2, 145–150	177.95	36	559	9.93	52.3	5.26	990	7.6	4.26	24.76	0.41	2.90
26X-3, 145–150	208.35	36	562	9.92	52.5	5.30	1001	7.5	4.36	25.36	0.39	2.26
29X-1, 145–150	234.35	36	559	9.84	53.4	5.43	1130	7.5	4.23	25.66	0.39	2.26
119-736C-												
8R-1, 145–150	266.15	36	560	10.15	53.4	5.26	1428	7.5	4.77	24.76	0.39	3.68
11R-3, 145–150	298.15	34	554	10.20	52.4	5.14	1939	7.3	4.31	24.45	0.40	5.48
14R-2, 145–150	325.75	35	545	10.05	52.0	5.18	1897	7.2	3.99	24.76	0.38	4.84
18R-2, 145–150	364.25	34	554	9.62	52.2	5.42	1943	7.2	3.60	25.06	0.39	4.96

to formulate a plausible explanation for sulfate depletion near the sediment/water interface and regeneration with increasing depth. A slight "hydrogen sulfide" odor was noticed in Sample 119-736A-16H-4, 145–150 cm, but no significant depletion in sulfate concentrations is observable in the data. The presence of high sulfate concentrations near the bottom of Hole 736A indicates either low levels of biological oxygen consumption and/or rapid diffusion of dissolved oxygen from the seafloor to relatively deep levels below the sediment/water interface.

Alkalinity values are approximately twice the average value of seawater (Fig. 13), which, considering the constancy of the pH data, indicates the addition of bicarbonate to the pore-water system, presumably by means of microbial degradation of organic matter.

Ammonium and Phosphate

Dissolved phosphate concentrations drop from a high of 16.69 μmol/L near the sediment/water interface to near average seawater values (about 5 μmol/L; Stumm and Morgan, 1970) at approximately 60 mbsf. This trend indicates that significant amounts of phosphate are produced near the sediment/water interface and that either phosphatic minerals are forming in the top 100 mbsf and/or phosphate is being lost to the water column.

Interstitial-water ammonium concentrations are significantly higher than average seawater values and increase with depth in Hole 736A (Fig. 13). The ammonium data imply that microbial degradation of organic matter continues to the bottom of Hole 736A, apparently under aerobic conditions.

ORGANIC GEOCHEMISTRY

Routine organic geochemical analyses were run on the first core from each hole and every third core where recovery permitted. The mud-line cores from Holes 736A and 736B were analyzed for comparison. The organic geochemistry program for Site 736 included (1) monitoring of hydrocarbon gases, (2) determining total organic carbon, and (3) characterizing organic matter. The methods and instruments used are described in the "Explanatory Notes" chapter.

Hydrocarbon Gases

Only the small-vial headspace procedure was used because no gas pockets were found at Site 736. Analysis was performed for approximately every 30 m of core to determine the concentrations of methane (C_1), ethane (C_2), and propane (C_3) dissolved in interstitial water and adsorbed on particles. C_2 or C_3 was not detected in any samples from Site 736. Core 119-736A-1H has 245 ppm (by volume) methane. All of the rest of the samples were at or near the 3-ppm mean level for laboratory air.

The absence of gas suggests that methanogenic bacteria were inactive during sedimentation at this site. Methanogens are anaerobes that are inhibited by sulfate ions (Claypool and Kvenvolden, 1983). Interstitial-water analysis showed that sulfate was relatively constant at approximately 24 mmol/L (see "Inorganic Geochemistry" section). This level was sufficient to inhibit the anaerobes.

Carbon Analysis

Total carbon and inorganic carbon were measured on the squeeze-cake samples left over from the interstitial-water study (see "Inorganic Geochemistry" section). The difference is the total organic carbon (TOC) (see "Explanatory Notes" chapter). Inorganic carbon was measured at several intervals from recovered core-catcher samples (Table 6 and Figs. 14 and 15). The low inorganic carbon at Site 736 coincides with the absence of calcareous organisms.

Organic carbon is high to moderate for diatomaceous sediments. The top 200 m of sediment has about 1% TOC. Below 200 mbsf, the values fall to 0.5% and steadily decrease downhole.

Rock-Eval Pyrolysis

Rock-Eval pyrolysis was also performed on the squeeze cakes left over from interstitial-water studies. The parameters measured and calculated are listed in Table 7 and shown in Figures 16–18.

BIOLOGY AND OCEANOGRAPHY

Phytoplankton: Living, Holocene, and Pleistocene Diatoms

Study of living species can add to the knowledge of fossil assemblages by clarifying which components of an existing ecosystem have been preserved in a death assemblage and by showing which life history stages of one species have been fossilized. On the other hand, the study of fossil assemblages can give direct evidence of evolutionary patterns for the systematist, plus provide a record of cyclic environmental phenomena. This interdisciplinary study considered both assemblies.

A small (10-cm mouth diameter) net with 20-μm mesh was deployed for living phytoplankton for 5 to 7 min per day at 1000 hr off the stern of the drillship in the effluent from the thrusters. Surface temperatures of 3.5°, 3.5°, 3.7°, and 4.0°C were recorded during the four sampling periods. Winds were 37,

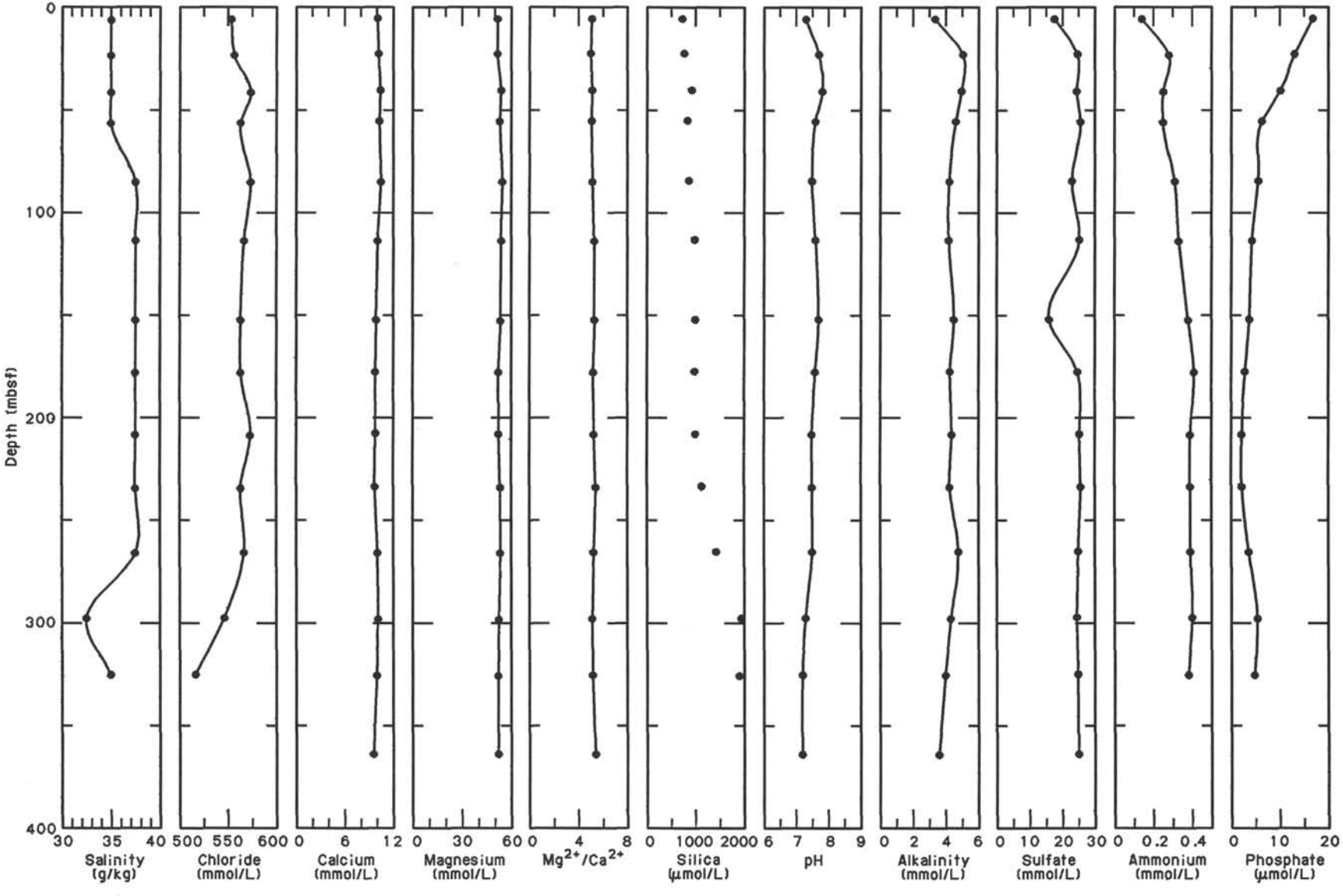

Figure 13. Salinity, chloride, calcium, magnesium, Mg^{2+}/Ca^{2+} ratio, silica, pH, alkalinity, sulfate, ammonium, and phosphate interstitial-water profiles, Site 736.

Table 6. Total carbon, inorganic carbon, organic carbon, and carbonate carbon, Site 736.

Sample (interval in cm)	Depth (mbsf)	Total carbon (%)	Inorganic carbon (%)	Organic carbon (%)	$CaCO_3$ (%)
736A-1H-4, 145-150	5.95	1.10	0.48	0.62	4.0
736B-1H-CC, 0-1	8.19		0.79		6.6
736B-1H-CC, 5-6	8.24		0.23		1.9
736A-1H-CC, 0-1	8.83		0.11		0.9
736A-2H-CC, 0-1	14.13		0.43		3.6
736B-2H-CC, 0-1	18.07		0.21		1.8
736A-3H-3, 145-150	22.95	0.91	0.04	0.87	0.3
736A-3H-CC, 0-1	24.63		0.18		1.5
736B-3H-CC, 0-1	27.37		0.09		0.8
736A-4H-CC, 0-1	32.61		0.04		0.3
736A-5H-CC, 0-1	38.05		0.02		0.2
736A-6H-2, 145-150	40.95	0.76	0.14	0.62	1.2
736A-6H-CC, 0-1	42.27		0.12		1.0
736A-7H-CC, 0-1	47.92		1.27		10.6
736A-8H-CC, 0-1	53.09		0.04		0.3
736A-9H-2, 145-150	55.95	1.49	0.06	1.43	0.5
736A-9H-CC, 0-1	58.76		0.64		5.3
736A-10H-CC, 0-1	66.14		0.06		0.5
736A-11H-CC, 0-1	73.00		1.17		9.8
736A-12H-CC, 0-1	79.16		0.60		5.0
736A-13H-4, 145-150	85.45	1.22	0.32	0.90	2.7
736A-13H-CC, 0-1	89.20		0.31		2.6
736A-14H-CC, 0-1	98.80		0.27		2.3
736A-15H-CC, 0-1	107.81		0.01		0.1
736A-16H-4, 145-150	113.95	0.61	0.04	0.57	0.3
736A-16H-CC, 0-1	117.50		0.17		1.4
736A-17X-CC, 0-1	120.71		0.09		0.8
736A-18X-CC, 0-1	127.57		0.15		1.3
736A-20H-4, 145-150	152.35	1.03	0.01	1.02	0.1
736A-20H-CC, 0-1	154.60		0.02		0.2
736A-21H-CC, 0-1	164.69		0.73		6.1
736A-22X-CC, 0-1	165.80		0.07		0.6
736A-23X-2, 145-150	177.95	1.28	0.12	1.16	1.0
736A-23X-CC, 0-1	178.20		0.20		1.7
736A-24X-CC, 0-1	186.47		0.08		0.7
736A-25X-CC, 0-1	194.40		0.25		2.1
736A-26X-3, 145-150	208.35	1.13	0.03	1.10	0.3
736A-26X-CC, 0-1	209.40		0.02		0.2
736C-2R-CC, 0-1	209.87		0.01		0.1
736A-27-CC, 0-1	214.48		0.37		3.1
736C-4R-CC, 0-1	226.18		0.50		4.2
736A-29X-1, 145-150	234.35	0.52	0.01	0.51	0.1
736A-29X-CC, 0-1	235.84		0.61		5.1
736C-5R-CC, 0-1	241.92		0.68		5.7
736A-30X-CC, 0-1	242.60		0.55		4.6
736C-6R-CC, 0-1	245.40		0.90		7.5
736C-7R-CC, 0-1	257.26		0.14		1.2
736C-8R-1, 145-150	266.15	1.24	0.84	0.40	7.0
736C-8R-CC, 0-1	267.49		0.84		7.0
736C-9R-4, 75-77	279.65		0.04		0.3
736C-9R-CC, 0-1	284.21		0.20		1.7
736C-10R-CC, 0-1	293.60		0.04		0.3
736C-11R-3, 145-150	298.15	0.36	0.04	0.32	0.3
736C-11R-CC, 0-1	300.03		0.05		0.4
736C-12R-CC, 0-1	303.91		0.04		0.3
736C-13R-CC, 0-1	322.60		0.03		0.3
736C-14R-2, 145-150	325.75	1.15	0.80	0.35	6.7
736C-14R-CC, 0-1	327.22		0.23		1.9
736C-15R-CC, 0-1	342.08		0.63		5.3
736C-16R-CC, 0-1	347.45		0.38		3.2
736C-17R-CC, 0-1	353.36		0.10		0.8
736C-18R-2, 145-150	364.25	0.49	0.20	0.29	1.7
736C-18R-CC, 0-1	366.07		0.14		1.2

27, 28, and 21 kt, respectively. The subantarctic summer flora was diverse, with long chains of vegetative cells and no resting spores noted (Table 8). The flora was increasing daily over the four-day period, as indicated by increasing phytoplankton abundance in the net.

In addition, dinoflagellates, a cold-water silicoflagellate (*Distephanus speculum*), gelatinous colonies of the prymnesiophyte *Phaeocystis*, and an acantharian were noted in the living community. Of particular interest are copepod fecal pellets, crowded

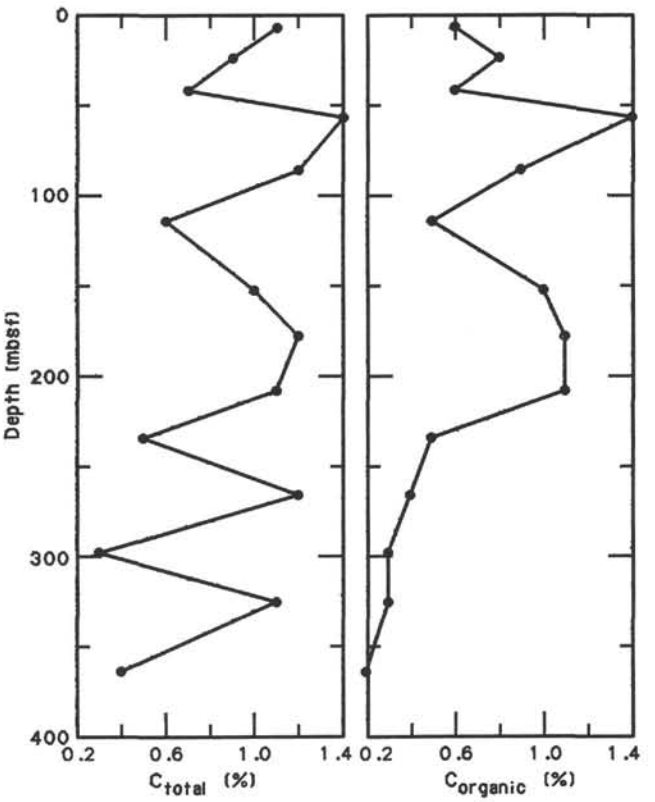

Figure 14. Total carbon (C_{total})and organic carbon ($C_{organic}$) from squeeze-cake and core-catcher sediment samples, Site 736.

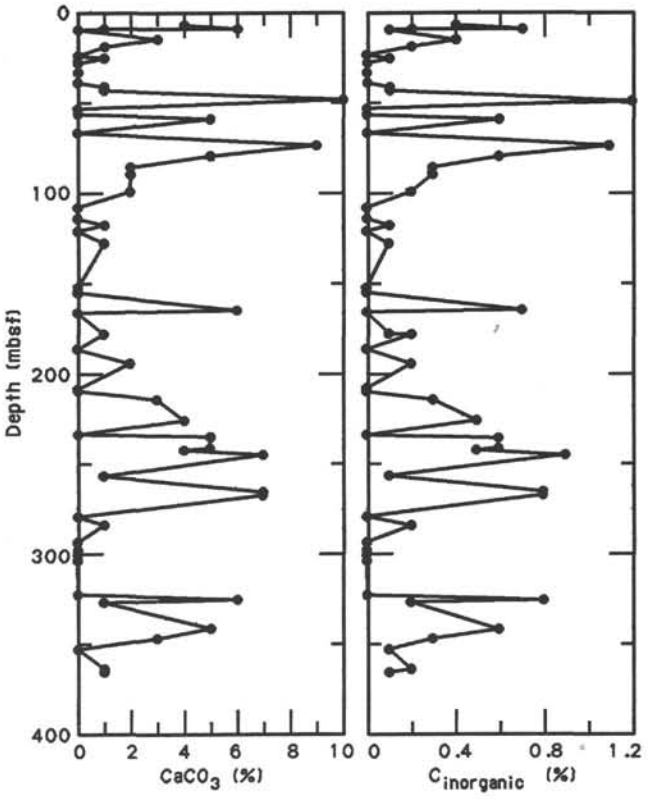

Figure 15. Percent calcium carbonate and inorganic carbon from squeeze-cake and core-catcher sediment samples, Site 736.

Table 7. Rock-Eval summary, Site 736.

Core, section, interval (cm)	Depth (mbsf)	Weight (g)	T_{max} (°C)	S1 (mg HC/g)	S2 (mg HC/g)	S3 (mg CO_2/g)	Productivity index	S2/S3	Pyrolysized carbon (0.08[S1 + S2])	TOC (wt%)	Hydrogen index (mg HC/g C_{org})	Oxygen index (mg CO_2/g C_{org})
119-736A-												
1H-4, 145–150	5.95	98.3	398	0.36	0.51	0.95	0.42	0.53	0.07	0.62	82	153
3H-3, 145–150	22.95	96.3	400	0.74	1.18	1.05	0.39	1.12	0.16	0.87	136	121
6H-2, 145–150	40.95	97.9	458	0.40	0.69	1.97	0.37	0.35	0.09	0.62	111	318
9H-2, 145–150	55.95	99.7	393	0.55	1.17	0.45	0.32	2.60	0.14	1.43	82	31
13H-4, 145–150	85.45	97.3	404	0.76	2.00	0.89	0.28	2.24	0.23	0.90	222	99
16H-4, 145–150	113.95	100.4	395	0.43	1.28	0.19	0.25	6.73	0.14	0.57	225	33
20H-4, 145–150	152.35	96.5	401	0.56	1.64	1.17	0.25	1.40	0.18	1.02	161	115
23X-2, 145–150	177.95	96.3	403	0.96	2.85	0.79	0.25	3.60	0.31	1.16	246	68
26X-3, 145–150	208.35	106.9	390	0.75	1.41	0.73	0.35	1.93	0.18	1.10	128	66
29X-1, 145–150	234.35	78.8	397	0.29	1.14	0.31	0.20	3.67	0.11	0.51	224	61
119-736C-												
8R-1, 145–150	266.15	102.0	400	0.27	0.32	0.85	0.47	0.37	0.04	0.40	80	213

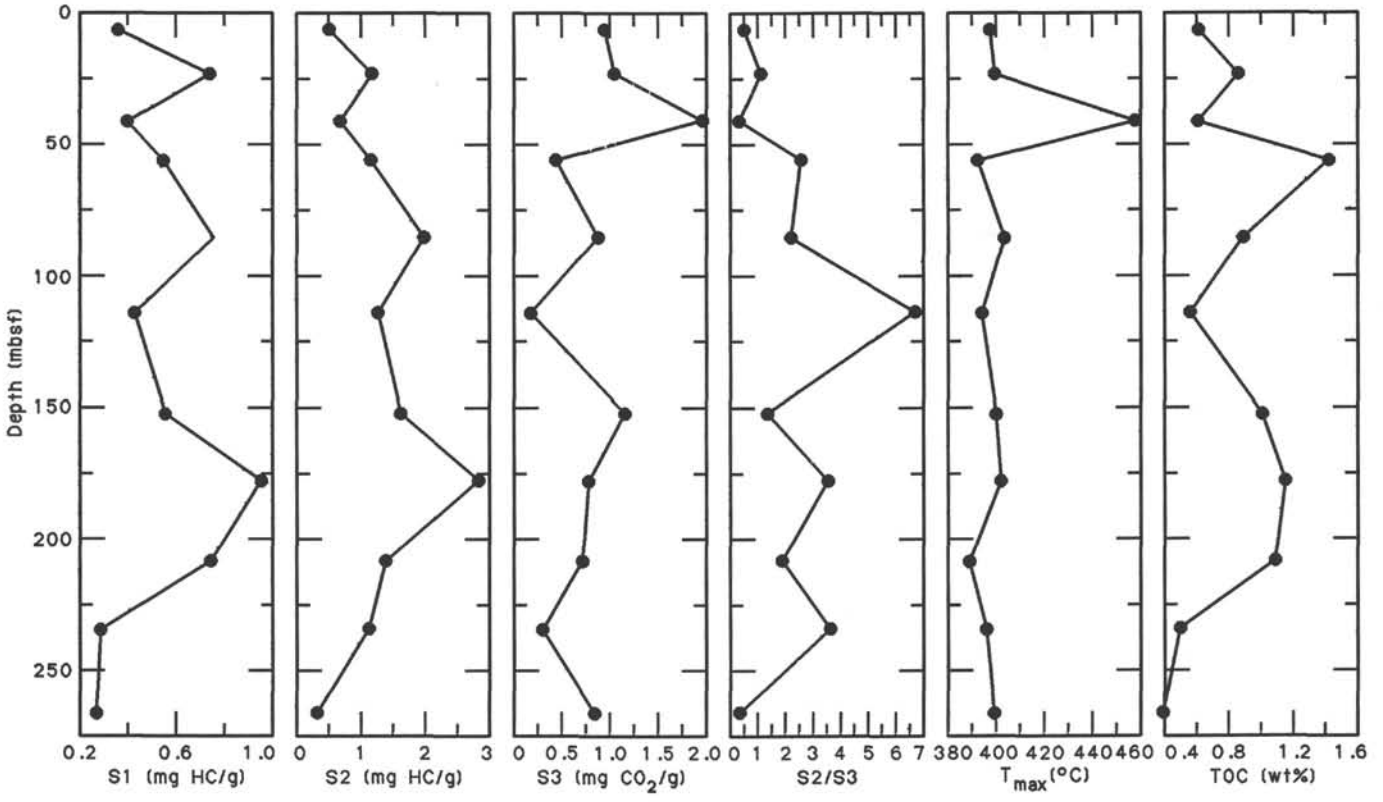

Figure 16. Comparison of Rock-Eval parameters S1, S2, S3, S2/S3, T_{max}, and TOC from Site 736. TOC was determined as the difference between total carbon and inorganic carbon.

with pennate diatom species that sink to the sediment more rapidly than individual cells. In most cases, a few pennate diatoms in the pellets were still pigmented and appeared alive. In a few cases, the pellets were crowded with reproducing cells.

Sediment was analyzed for diatom species from the mud line and from core catchers from Cores 119-736A-1H through 119-736A-17X and 119-736B-1H through 119-736B-3H. Additional species not found in the living plankton are listed in Table 9. A sediment assemblage has been averaged over time (depending on sedimentation rate, in this case estimated at 80 m/m.y.) and over space (depending on currents) in contrast to the short time/space scale represented by the samples of the living phytoplankton. Thus, some species found in the fossil assemblage analyzed from the Holocene and Pleistocene sediments may grow in other seasons and were not found in these summer samples.

Easily dominating both the living plankton and the assemblage in the sediment was the pennate diatom genus *Nitzschia*. In the sediment, the dominant species was *Nitzschia kerguelensis* from the group of species of the genus with ribbon-shaped colonies; in the plankton, the dominant form was needle-shaped *Nitzschia* species from the group forming colonies with overlapping tips. Also well represented with several species was the centric diatom genus *Thalassiosira*. *Chaetoceros* was well represented in the plankton; in the sediment, *Chaetoceros neglectus* resting

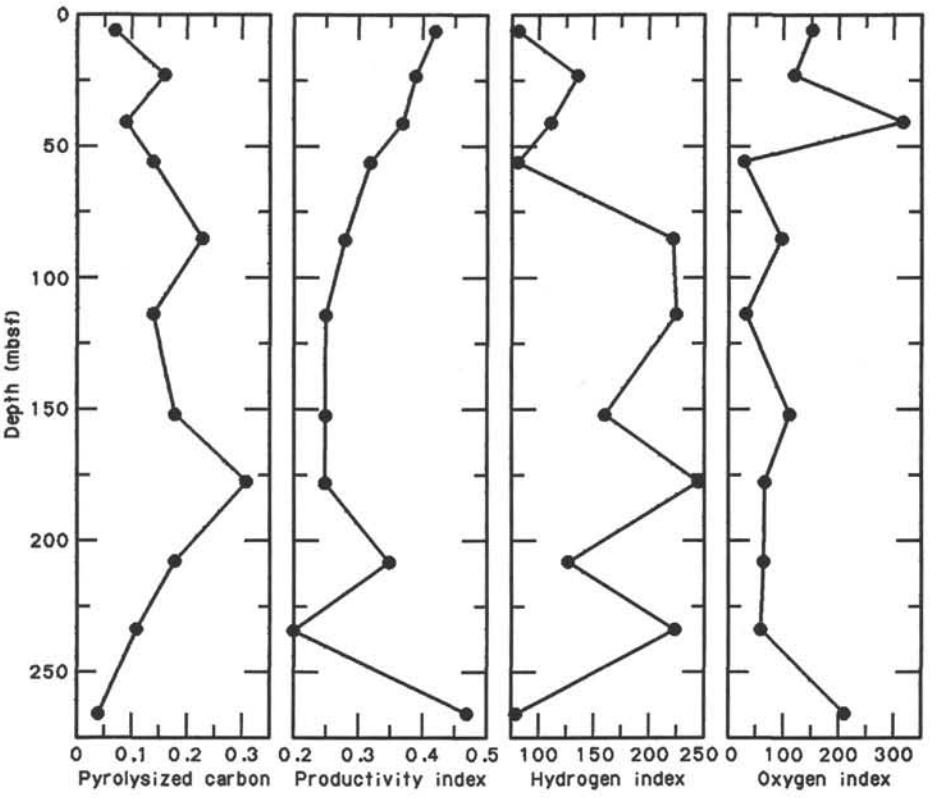

Figure 17. Comparison of Rock-Eval parameters pyrolysized carbon, productivity index, hydrogen index, and oxygen index, Site 736.

spores were present, in addition to a few resting spores from an unknown species of *Chaetoceros* and from *Chaetoceros radicans*.

Evidently frustules from only certain selected species both reach the ocean floor and are preserved in the fossil assemblage. The proportion of empty cells has not been found to increase appreciably with depth in the euphotic zone of the Weddell Sea (Fryxell and Kendrick, 1988). As the numbers of living cells generally decrease with depth, the numbers of empty (dead) cells also decrease. Apparently no steady rain of cells reaches the sediment. The heavily silicified resting spores or vegetative thecae seen in the sediment could well be deposited in pulses following periods of abundant growth. Fecal pellets sink rapidly out of the water column and could also be a major contributor to sediments.

PHYSICAL PROPERTIES

The objectives of the physical-properties program at Site 736 were (1) to add to the limited data base of geotechnical and other physical properties of high-latitude sediments (the site is south of the Antarctic Convergence), particularly those containing abundant biogenic silica, and (2) to provide reference data for the geophysical and stratigraphic evaluation of the sedimentary section at the site.

Physical properties evaluated were (1) index properties, (2) undrained shear strength, (3) thermal conductivity, and (4) compressional-wave velocity. General techniques and laboratory procedures are discussed in the "Explanatory Notes" chapter.

Three holes (736A, 736B, and 736C) were drilled at the site with APC, XCB, and RCB. The degree of core disturbance, as observed both visually and in the physical properties, increased slightly from APC to XCB cores and significantly in RCB cores.

All physical-properties data, except temperature, are presented in Figure 19 and Tables 10 through 14. Temperature measurements are presented in Figures 20 and 21 and Table 15.

Index Properties

Values of water content, porosity, bulk density, and grain density can be subdivided into two geotechnical units, G1 and G2, corresponding to a change from APC/XCB to RCB coring from Holes 736A and 736B to Hole 736C. Hence, the division is mainly a function of core disturbance. The upper part of the sedimentary section, above 235 mbsf, shows a slight overall decrease in water content, whereas porosity, bulk density, and grain density stay relatively constant, despite a large local scatter (the data have not been filtered for bad data points). This is somewhat anomalous, as porosity would be expected to decrease and bulk density to increase with increasing overburden/decreasing water content. This anomaly is most likely a consequence of the lithology. The sediment is essentially a diatom ooze throughout the entire section ("Lithostratigraphy and Sedimentology" section). Diatom ooze will maintain a relatively open but strong structure that prevents large downcore changes. An increase in the content of volcanic fragments toward the top of the core—fragments that mostly consist of pumice—may also contribute to the observed trends.

Generally, the index properties are correlative (Fig. 19 and Table 10). Decreases in water content correspond to intervals of decreasing porosity and increasing bulk density. The positive correlation between grain and bulk density is unusual in that typically no correspondence appears between grain density and index properties. This correlative relationship is probably a consequence of the diatomaceous lithology, which is also the cause of the generally low density values. Biogenic silica has a low density of 2.02 g/cm^3 (Barker, Kennett, et al., 1988).

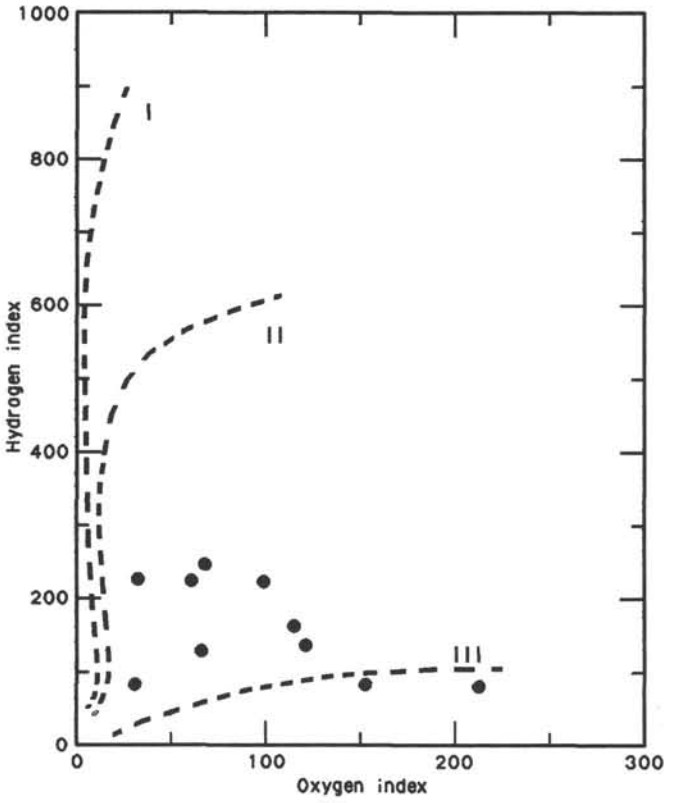

Figure 18. Hydrogen and oxygen indices obtained from Rock-Eval pyrolysis of squeeze-cake sediment samples from Site 736 plotted on a van Krevelen-like diagram (Tissot and Welte, 1984).

The lower part of the section, RCB cored in Hole 736C, shows a return to normal, expected trends of decreasing porosity and water content with depth and slightly raised but fairly constant values of bulk density. This is rather surprising in view of the fact that visual examination of the split cores revealed extensive disturbance: bedding deformation due to friction along core liners, bedding plane separations, and, in the deepest sections, liquefaction of the recovered material.

Bulk density measured by the GRAPE on whole-round core sections shows the same trends as for the gravimetrically determined values. Relatively high values in the upper 50–60 m are due mostly to the content of volcanic fragments, which were not present in the samples measured gravimetrically. Furthermore, the large scatter toward higher values is caused by gravelly material that fell into the hole and concentrated in the core tops. The most distinct feature in the GRAPE data is the more concentrated values of Hole 736C (RCB cores), which again are slightly raised relative to the upper part of the section. In general, the GRAPE values are approximately 0.05 to 0.1 g/cm^3 higher than those measured on discrete samples. The higher GRAPE values probably resulted from measuring whole-round cores, which include coarser material not included in the small discrete samples.

Undrained Shear Strength

The variability of undrained shear-strength values above 100 mbsf reflects variations in index properties in this interval and shows an overall trend of slightly increasing values with depth. Both the vane shear and the fall cone measurements show the same trend and local variations (an exception is the high values of cone shear strength at 150–170 mbsf that are not apparent in the vane shear strength), but the values of the fall cone measurements are generally higher than those of the vane shear (Fig. 19 and Tables 11 and 12). The scatter is also larger for the former device. A decrease occurs in the shear-strength trend from 110 to 210 mbsf. This interval corresponds to the change from APC to RCB coring with poor recovery and probably reflects sample disturbance. The high values in cone shear-strength values around

Table 8. Species found in living plankton, Site 736.

[a]*Asteromphalus hookeri*
Asteromphalus parvulus
[a]*Azpeitia tabularis*
Chaetoceros castracanei
Chaetoceros constrictus
Chaetoceros convolutus
Chaetoceros curvisetus
Chaetoceros pendulus
Corethron inerme
[b]*Dactyliosolen antarcticus*
[c]*Eucampia antarctica* (two kinds of spiraling chains)
Navicula directa
Nitzschia closterium
Nitzschia heimii
[d]*Nitzschia kerguelensis*
Nitzschia turgidula
Nitzschia turgiduloides
[c]*Odontella weissflogii* vegetative cells
Porosira pseudodenticulata
Rhizosolenia alata (long, straight chains)
Rhizosolenia chunii
Rhizosolenia cylindrus
Rhizosolenia hebetata f. *semispina* (also *bidens*)
Rhizosolenia simplex
[a]*Thalassionema nitzschioides*
Thalassiosira gravida (gelatinous colonies)
[a]*Thalassiosira lentigenosa*
[a]*Thalassiosira tumida*
Thalassiosira maculata?
[a]*Thalassiothrix antarctica*?
Tropidoneis antarctica

[a] Also found in sediment.
[b] Also found only in the heavily silicified bands in sediment.
[c] Winter stage found in sediment.
[d] Three forms found in sediment.
[e] Resting spores found in sediment.

Table 9. Species found only in the sediment, Site 736.

Actinocyclus actinochilus
Actinocyclus ingens
Asteromphalus hyalina
Azpeitia endoi?
Chaetoceros sp. (resting spore)
Cocconeis fasciolata
Coscinodiscus elliptopora
Coscinodiscus oculoides
Coscinodiscus spp.
Nitzschia angulata
Nitzschia curta
Nitzschia obliquecostata
Nitzschia panduriformis
Nitzschia ritscheri
Nitzschia separanda
Paralia sulcata
Porosira glacialis (resting spore)
Rouxia isopolica Schrader (extinct)
Thalassiosira ambigua
Thalassiosira australis
Thalassiosira gracilis f. *gracilis*
Thalassiosira gracilis f. *expecta*
Thalassiosira oliverana
Thalassiosira scotia (resting spore)
Thalassiosira trifulta
Thalassiosira "sp. 10" sensu Schrader
Thalassiosira sp. cf. *lentiginosa*

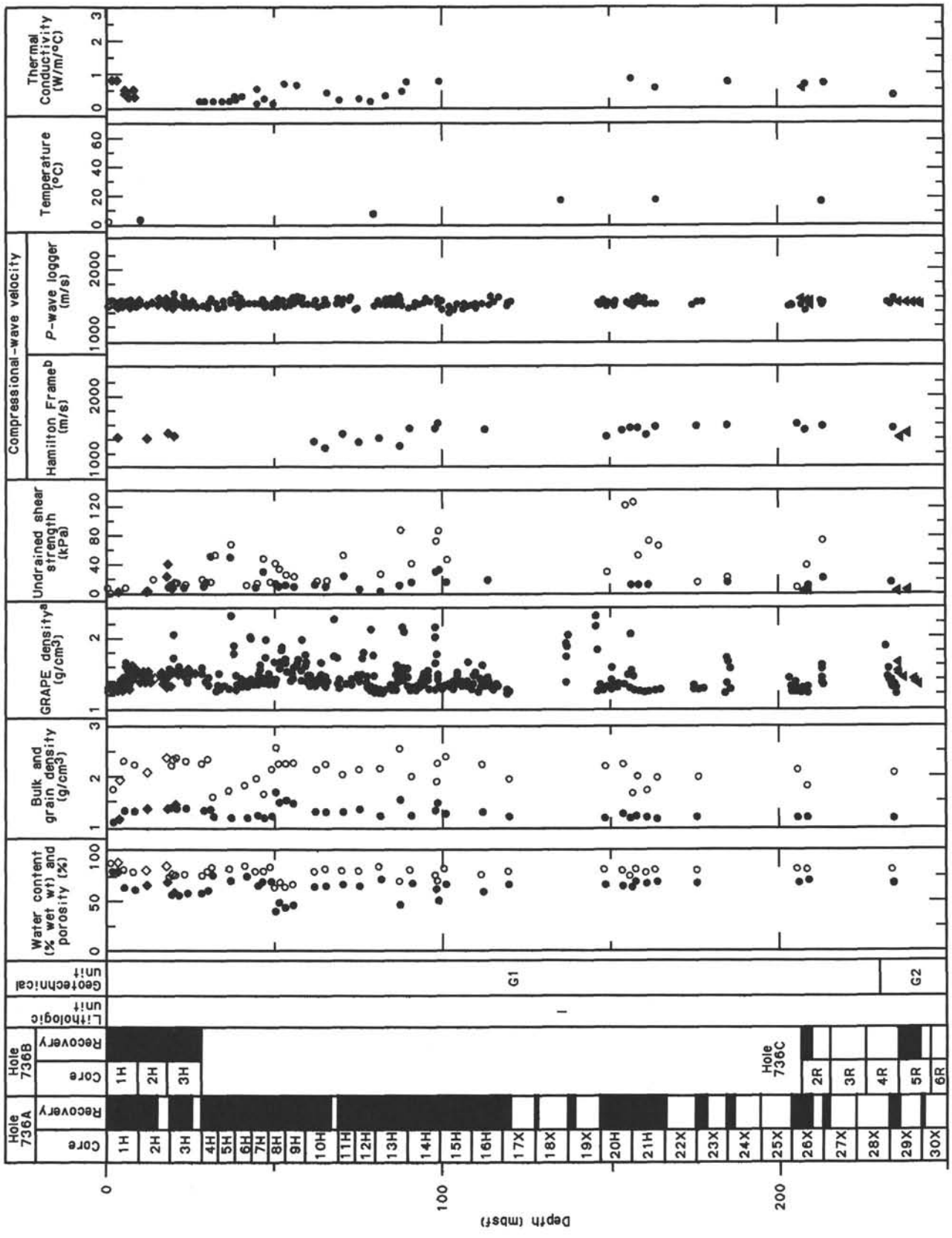
Hole 736A
Core
Recovery
Hole 736B
Core
Recovery
Lithologic Unit
Geotechnical Unit
Water content (% wet wt) and porosity (%)
Bulk and grain density (g/cm3)
GRAPE density (g/cm3)
Undrained shear strength (kPa)
Compressional-wave velocity
Hamilton Frame (m/s)
P-wave logger (m/s)
Temperature (°C)
Thermal Conductivity (W/m/°C)
Depth (mbsf)
G1
G2
I
Hole 736C

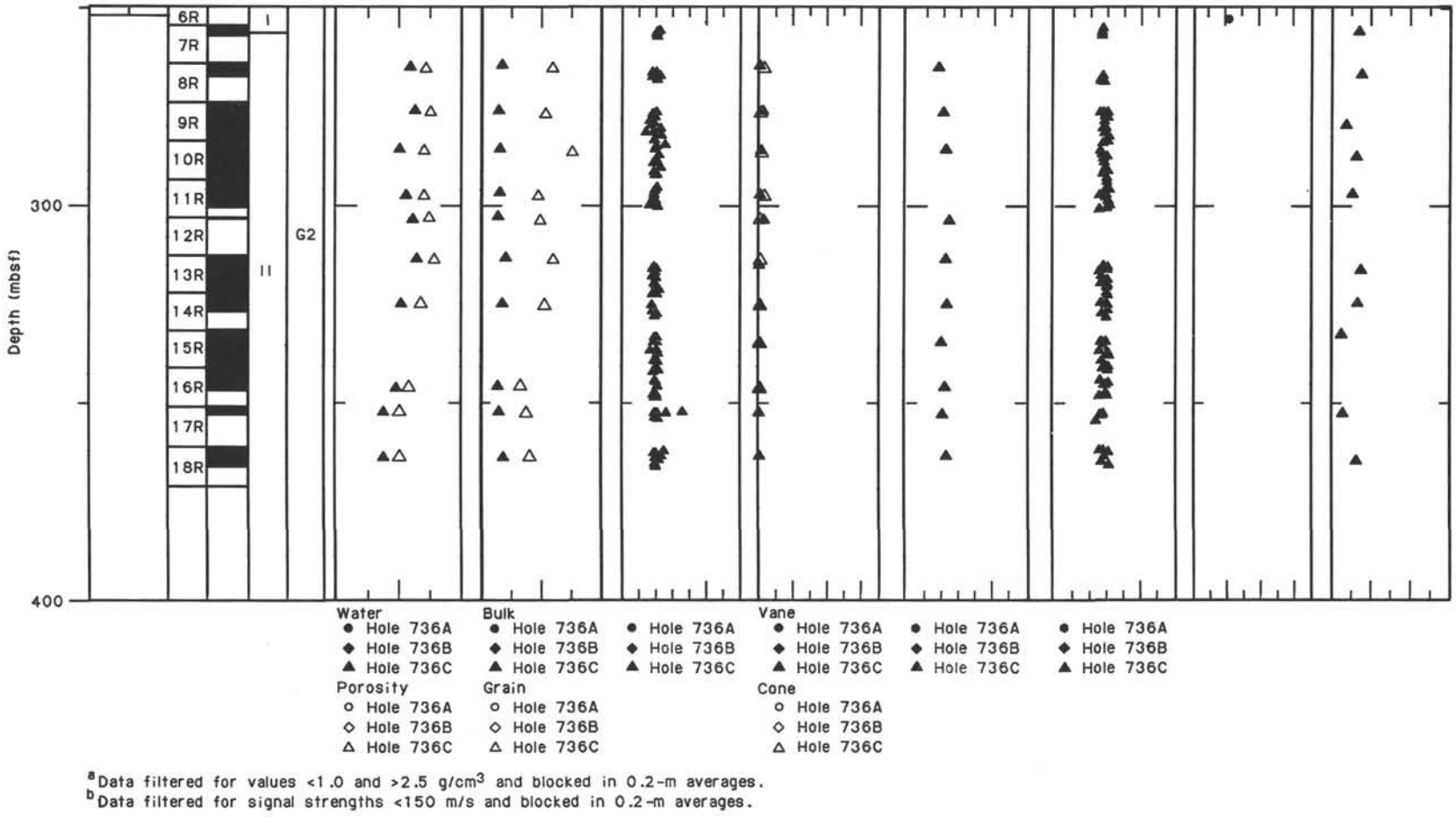

[a] Data filtered for values <1.0 and >2.5 g/cm^3 and blocked in 0.2-m averages.
[b] Data filtered for signal strengths <150 m/s and blocked in 0.2-m averages.

Figure 19. Physical-property profiles, Site 736.

Table 10. Index properties of water content, porosity, bulk density, dry-bulk density, and grain density, Site 736.

Core, section, interval (cm)	Depth (mbsf)	Water (%)	Porosity (%)	Bulk density (g/cm^3)	Dry-bulk density (g/cm^3)	Grain density (g/cm^3)
119-736A-						
1H-2, 75	2.24	79.59	87.46	1.11	0.23	1.74
1H-4, 101	5.50	63.86	80.22	1.33	0.48	2.30
1H-6, 111	8.60	61.86	78.31	1.32	0.51	2.23
2H-4, 111	13.73	78.35	83.66	1.08	0.23	1.31
3H-1, 96	19.45	56.98	74.45	1.40	0.60	2.21
3H-2, 100	20.99	56.74	75.52	1.38	0.60	2.36
3H-4, 58	23.57	58.23	76.17	1.39	0.58	2.30
4H-1, 98	28.97	58.49	75.93	1.35	0.56	2.25
4H-2, 98	30.47	61.16	78.63	1.37	0.53	2.34
4H-3, 91	31.90	76.39	84.16	1.22	0.29	1.59
5H-3, 95	36.92	71.58	81.50	1.20	0.34	1.72
6H-3, 83	41.82	75.38	85.09	1.20	0.30	1.83
7H-2, 68	45.17	66.17	79.35	1.25	0.42	1.96
7H-3, 93	46.90	70.86	80.24	1.20	0.35	1.64
8H-1, 137	49.36	70.76	83.91	1.22	0.36	2.14
8H-2, 131	50.80	40.84	63.86	1.71	1.01	2.59
8H-3, 106	52.05	49.66	68.91	1.51	0.76	2.26
9H-1, 84	53.83	45.28	64.83	1.55	0.85	2.25
9H-3, 20	56.19	46.69	66.26	1.49	0.80	2.26
10H-3, 65	62.62	64.17	79.35	1.33	0.48	2.15
10H-5, 86	65.85	66.13	81.48	1.32	0.45	2.25
11H-2, 81	70.80	67.14	80.73	1.32	0.43	2.04
12H-2, 76	75.75	65.88	80.51	1.37	0.47	2.14
13H-2, 104	82.03	72.73	85.35	1.24	0.34	2.17
13H-6, 86	87.85	47.63	69.74	1.56	0.82	2.56
14H-2, 81	91.30	68.83	81.67	1.26	0.39	2.01
14H-7, 71	98.70	62.90	76.33	1.36	0.50	1.90
15H-1, 77	99.26	51.40	70.54	1.49	0.72	2.28
15H-3, 73	101.57	67.21	83.15	1.29	0.42	2.41
16H-4, 93	112.59	60.12	77.08	1.32	0.53	2.24
17X-1, 96	120.45	67.51	80.38	1.23	0.40	1.96
20H-2, 127	149.16	66.99	81.65	1.21	0.40	2.19
20H-6, 40	154.29	66.00	81.31	1.28	0.44	2.24
21H-1, 81	156.70	65.07	75.84	1.20	0.42	1.67
21H-2, 104	158.43	70.25	82.69	1.24	0.37	2.01
21H-4, 111	161.48	68.41	79.01	1.20	0.38	1.72
21H-6, 94	164.33	69.54	81.88	1.19	0.36	1.97
23X-2, 15	176.64	68.44	81.30	1.21	0.38	1.99
24X-1, 90	185.49	37.27	60.68	1.66	1.04	2.63
26X-2, 86	206.25	69.32	82.90	1.20	0.37	2.14
26X-4, 71	209.10	70.47	81.31	1.20	0.35	1.80
29X-2, 28	234.67	67.98	81.51	1.18	0.38	2.07
119-736B-						
1H-3, 76	3.75	79.67	88.47	1.17	0.24	1.91
2H-3, 77	12.16	65.94	80.18	1.37	0.47	2.09
2H-CC, 11	18.17	70.16	84.83	1.38	0.41	2.37
3H-2, 76	20.15	58.21	76.41	1.43	0.60	2.34
119-736C-						
8R-1, 73	265.40	57.97	74.87	1.33	0.56	2.17
9R-2, 76	276.65	64.42	78.78	1.27	0.45	2.05
10R-2, 79	286.27	53.11	73.78	1.30	0.61	2.50
11R-3, 83	297.50	58.91	73.38	1.30	0.54	1.92
12R-1, 28	303.65	64.59	78.21	1.25	0.44	1.96
13R-1, 75	313.84	68.22	82.40	1.39	0.44	2.17
14R-2, 83	325.10	54.68	70.84	1.34	0.61	2.02
16R-3, 96	345.93	49.88	61.77	1.26	0.63	1.62
17R-1, 83	352.40	40.34	53.70	1.28	0.77	1.72
18R-2, 73	363.50	39.28	53.22	1.36	0.82	1.77

150–170 mbsf were measured in two APC cores that were taken within the RCB coring session. However, downcore-decreasing shear-strength values have been reported from other siliceous sections (Eldholm, Thiede, et al., 1987); thus, a lithologic cause can not be excluded.

Shear-strength values below about 210 mbsf are very low, reflecting the disturbance associated with rotary coring in these sediments. Values of shear strength for Holes 736A and 736C overlap from about 200 to 225 mbsf. These data suggest that shear strength, and presumably index properties as well, is little affected by XCB recovery (165–242 mbsf, Hole 736A) whereas RCB recovery (207 mbsf to total depth, Hole 736C) results in complete remolding of the sediment.

Compressional-Wave Velocity

Compressional-wave velocities, which were determined with the Hamilton Frame and *P*-wave logger, show generally comparable but somewhat different values and trends (Fig. 19). Both

Table 11. Undrained shear strength from vane measurements, Site 736.

Core, section, interval (cm)	Depth (mbsf)	Undrained shear strength (kPa)
119-736A-		
1H-1, 20	0.20	6.2
3H-1, 95	19.45	9.1
3H-2, 105	21.05	8.7
3H-4, 57	23.57	7.0
4H-1, 92	28.92	9.1
4H-2, 94	30.44	15.3
4H-3, 88	31.88	51.5
5H-3, 96	36.96	49.7
7H-2, 70	45.20	8.7
7H-3, 88	46.88	30.0
8H-2, 128	50.78	14.3
8H-3, 103	52.03	10.6
9H-1, 76	53.76	11.6
9H-3, 18	56.18	9.1
10H-3, 67	62.67	12.8
10H-5, 85	65.85	9.5
11H-2, 80	70.80	24.2
12H-2, 75	75.75	5.4
13H-2, 103	82.03	3.3
13H-6, 85	87.85	11.4
14H-2, 80	91.30	15.1
14H-7, 70	98.70	31.0
15H-1, 76	99.26	32.7
15H-3, 70	102.20	16.1
16H-4, 90	113.40	18.6
21X-1, 82	156.72	11.4
21X-2, 99	158.39	11.2
21X-4, 108	161.48	11.4
24X-1, 93	185.53	14.5
26X-4, 73	209.13	10.8
27X-1, 55	214.05	20.7
29X-2, 28	234.68	15.5
119-736B-		
1H-3, 75	3.75	0.6
2H-3, 76	12.16	1.4
2H-CC, 10	18.17	23.4
3H-2, 75	20.15	6.6
119-736C-		
2R-2, 80	209.20	2.1
5R-1, 123	236.93	1.2
5R-3, 83	239.53	3.1
8R-1, 70	265.40	0.4
9R-2, 75	276.65	3.3
10R-2, 77	286.27	2.3
11R-3, 80	297.50	0.8
12R-1, 25	303.65	5.2
13R-2, 74	315.34	0.2
14R-2, 80	325.10	0.2
15R-2, 86	334.76	0.2
16R-3, 83	345.83	0.2
17R-1, 80	352.40	0.2
18R-2, 70	363.50	0.2

Table 12. Undrained shear strength from fall cone measurements, Site 736.

Core, section, interval (cm)	Depth (mbsf)	Undrained shear strength (kPa)
119-736A-		
1H-2, 65	2.15	0.8
1H-4, 100	5.50	6.1
2H-4, 100	13.63	19.0
3H-1, 92	19.42	11.0
3H-2, 99	20.99	13.0
3H-4, 59	23.59	11.0
4H-1, 93	28.93	19.0
4H-2, 98	30.48	15.0
4H-3, 91	31.91	53.0
5H-3, 98	36.98	68.0
6H-3, 82	41.82	12.0
7H-2, 67	45.17	15.0
7H-3, 91	46.91	48.0
8H-1, 139	49.39	16.0
8H-2, 132	50.82	42.0
8H-3, 105	52.05	34.0
9H-1, 82	53.82	26.0
9H-3, 16	56.16	24.0
10H-3, 67	62.67	17.0
10H-5, 85	65.85	18.0
11H-2, 80	70.80	53.0
12H-2, 75	75.75	8.9
13H-2, 103	82.03	27.0
13H-6, 85	87.85	88.0
14H-2, 80	91.30	42.0
14H-7, 70	98.70	74.0
15H-1, 76	99.26	88.0
15H-3, 70	102.20	48.0
16H-4, 90	113.40	21.0
20H-2, 128	149.18	30.0
20H-6, 39	154.29	123.0
21H-1, 80	156.70	127.0
21H-2, 103	158.43	53.0
21H-4, 115	161.55	74.0
21H-6, 94	164.34	67.0
23X-2, 10	176.60	16.0
24X-1, 90	185.50	22.0
26X-2, 83	206.23	9.0
26X-4, 71	209.11	39.0
27X-1, 60	214.10	74.0
29X-2, 22	234.62	19.0
119-736B-		
1H-3, 75	3.75	0.8
2H-3, 76	12.16	2.7
2H-CC, 10	18.17	41.0
3H-2, 75	20.15	15.0
119-736C-		
2R-2, 83	209.23	3.3
5R-1, 123	236.93	2.3
5R-3, 85	239.55	4.5
8R-1, 70	265.40	6.6
9R-2, 75	276.65	2.7
10R-2, 77	286.27	4.2
11R-3, 80	297.50	7.0
12R-1, 25	303.65	2.5
13R-1, 74	313.84	2.1
14R-2, 80	325.10	1.9
15R-2, 86	334.76	1.3
16R-3, 93	345.93	0.8
17R-1, 80	352.40	1.3

of the instruments measure velocity parallel to bedding. Differences, therefore, are not due to directional anisotropy. *P*-wave-logger values are characterized by a slight but steady trend toward increasing values with depth. No break is apparent in this trend between Holes 736A and 736C. Because of operational problems, Hamilton Frame measurements were not started before 62 mbsf in Hole 736A, and the low values first recorded may be erroneous (Table 13). However, the data show a distinct increase with depth to around 200 mbsf. Hamilton Frame data below 200 mbsf are anomalous and are obviously the result of severe core disturbance caused by rotary drilling below this depth. *P*-wave-logger results seem to be less affected by the disturbance. However, this may be only apparent, and the consistent trend could be caused by the partly liquified sediments being compacted inside the liner when placed vertically in the GRAPE/P-wave-logger frame. In general, the velocities are low for the entire section. This is most likely a consequence of sediment type.

Table 13. Compressional-wave velocity determined with the Hamilton Frame, Site 736.

Core, section, interval (cm)	Depth (mbsf)	Compressional-wave velocity (m/s)
119-736A-		
10H-3, 70–73	62.70	1363
10H-5, 80–83	65.80	1263
11H-2, 80–83	70.80	1468
12H-2, 75–77	75.75	1349
13H-2, 105–107	82.05	1411
13H-6, 86–88	87.86	1305
14H-2, 80–83	91.30	1532
14H-7, 70–73	98.70	1534
15H-1, 76–79	99.26	1609
16H-4, 90–93	113.40	1540
20H-2, 129–132	149.19	1427
20H-6, 40–43	154.30	1516
21H-1, 76–79	156.66	1540
21H-2, 106–109	158.46	1544
21H-6, 95–98	164.35	1566
23X-2, 10–13	176.60	1569
24X-1, 87–90	185.47	1584
26X-2, 80–83	206.20	1602
26X-4, 68–71	209.08	1516
27X-1, 60–63	214.10	1573
29X-2, 31–34	234.71	1532
119-736B-		
1H-3, 75–78	3.75	1412
2H-3, 76–79	12.16	1402
2H-CC, 10–13	18.17	1459
3H-2, 75–78	20.15	1440
119-736C-		
5R-1, 115–118	236.85	1398
5R-3, 78–81	239.48	1465
8R-1, 70–73	265.40	1369
9R-2, 75–78	276.65	1426
10R-2, 77–79	286.27	1461
12R-1, 25–28	303.65	1500
13R-1, 74–76	313.84	1454
14R-2, 80–83	325.10	1466
15R-2, 86–89	334.76	1403
16R-3, 80–83	345.80	1445
17R-1, 80–83	352.40	1422
18R-2, 70–73	363.50	1462

Thermal Conductivity

Thermal-conductivity values were measured on APC, XCB, and RCB cores and show high variability that is largest with the RCB cores (Fig. 19 and Table 14). During measurement, the thermal-conductivity instrument showed a relatively large temperature drift gradient. Only points where this gradient exceeds 1.0°C/min were removed, whereas the instrument manual recommends that values greater than 0.01°C/min should not be used. High drift gradients may explain why many conductivity values are lower than 0.59 W/m/°C, the conductivity of water at ambient conditions, and why the thermal-conductivity data seemingly show low correspondence to the other physical parameters.

The conductivity values have an apparent bimodal distribution (0.2–0.5 and 0.65–0.85). The lower values are unrealistically low, but the upper values, even though of relatively small magnitude, are similar to values recorded at other Leg 119 sites on the Kerguelen Plateau. Bimodal distribution of thermal conductivity values has been related to systematic variations in mineral components (Matsuda and Von Herzen, 1986). However, we suspect that the lower set of values at Site 736 is erroneous and is due in large part to insufficient laboratory "stabilization time" for the cores before measuring the conductivities.

Table 14. Thermal conductivity, Site 736.

Core, section, interval (cm)	Depth (mbsf)	Thermal conductivity (W/m/°C)
119-736A-		
4H-1, 89	28.89	0.215
4H-3, 91	31.91	0.201
5H-2, 30	34.80	0.241
5H-4, 30	37.80	0.257
6H-1, 87	38.87	0.393
7H-2, 20	44.70	0.660
7H-2, 100	45.50	0.184
7H-4, 20	47.70	0.322
8H-1, 100	49.00	0.197
9H-1, 80	53.80	0.792
9H-3, 80	56.80	0.701
10H-5, 70	65.70	0.487
11H-1, 80	69.30	0.251
12H-2, 70	75.70	0.349
12H-4, 70	78.70	0.191
13H-3, 80	83.30	0.407
13H-6, 80	87.80	0.515
14H-1, 100	90.00	0.807
15H-1, 100	99.50	0.816
21H-1, 100	156.90	0.905
21H-6, 100	164.40	0.627
24X-1, 100	185.60	0.803
26X-4, 50	208.90	0.733
27X-1, 50	214.00	0.760
29X-2, 80	235.20	0.416
119-736B-		
1H-2, 50	2.00	0.870
1H-4, 100	5.50	0.517
1H-5, 70	6.70	0.554
1H-5, 130	7.30	0.381
119-736C-		
2R-1, 100	207.90	0.612
7R-1, 80	255.80	0.718
8R-2, 80	267.00	0.799
9R-4, 80	279.70	0.392
10R-3, 80	287.80	0.679
11R-3, 80	297.50	0.553
13R-3, 75	316.85	0.770
14R-2, 75	325.05	0.683
15R-1, 75	333.15	0.284
17R-1, 75	352.35	0.328
18R-3, 50	364.80	0.692

Thermal conductivities for poorly consolidated sediments are greatly dependent on porosity and water content (Lachenbruch and Marshall, 1966). The high porosity values (80%) in the diatom oozes at Site 736 probably explain the small conductivity values that were not biased by stabilization time (Fig. 19). These values, like those of the diatomaceous oozes of Site 737, average about 0.7 W/m/°C.

Temperature and Heat Flow

Temperature measurements were made at five sub-bottom depths in Hole 736A and at one depth in Hole 736C using the Uyeda probe and standard operational procedures (see "Explanatory Notes" chapter). The results are listed in Table 15 and shown for each measurement in Figure 20. Temperature equilibration curves are given in Figure 21. A summary plot of temperature vs. depth and measured conductivity values for Site 736 is shown in Figure 19.

The temperature measurements at Site 736 are generally good. For some measurements, however, ship surge of up to 4–7 m probably caused the probe to be extracted and reinserted during the measurements, thereby adding irregularities to the tempera-

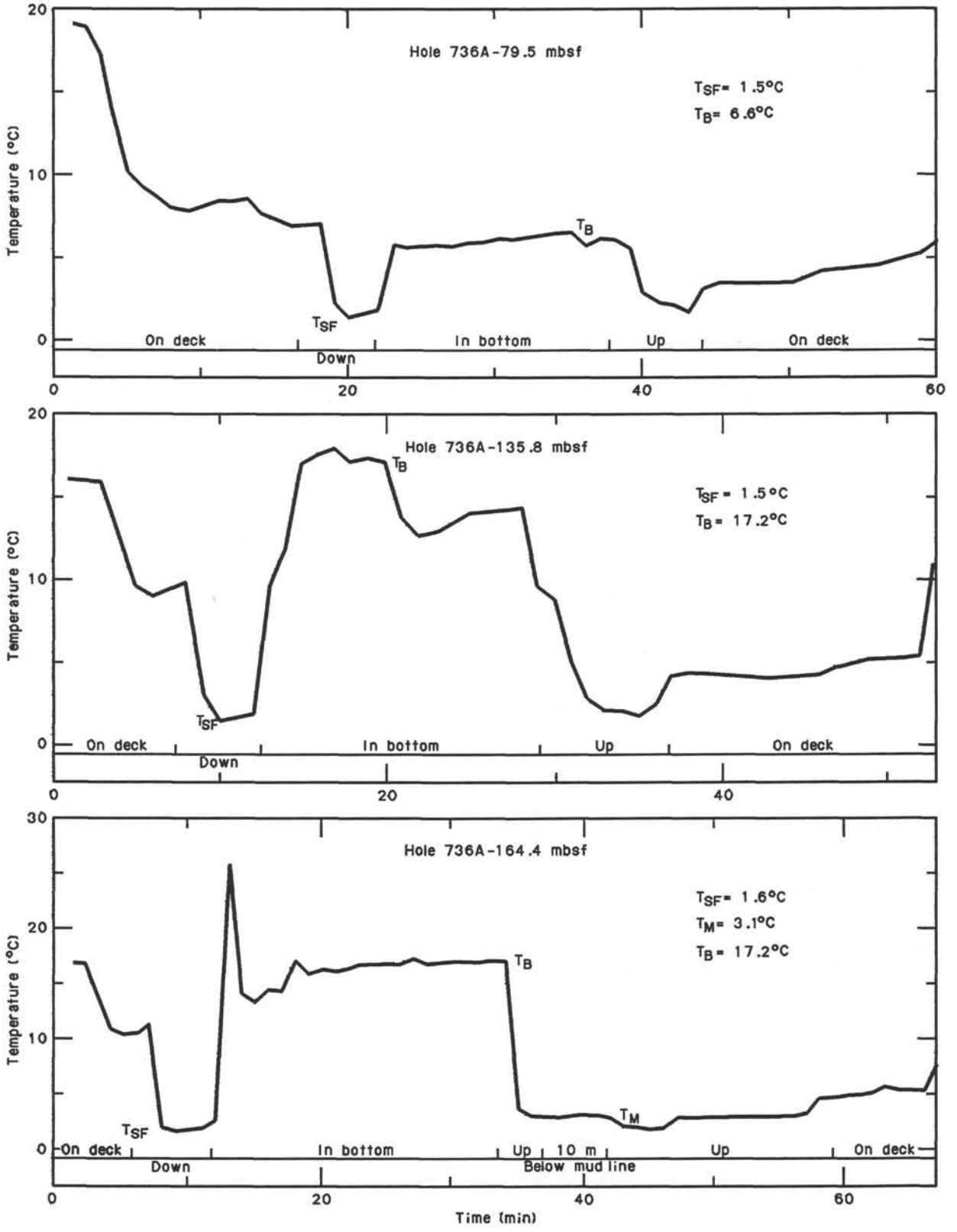

Figure 20. Temperature vs. measurement time for six Uyeda probe deployments in Holes 736A and 736C. See Table 15 for critical temperature points T_{SF}, and T_B. T_M = temperature at 10 mbsf.

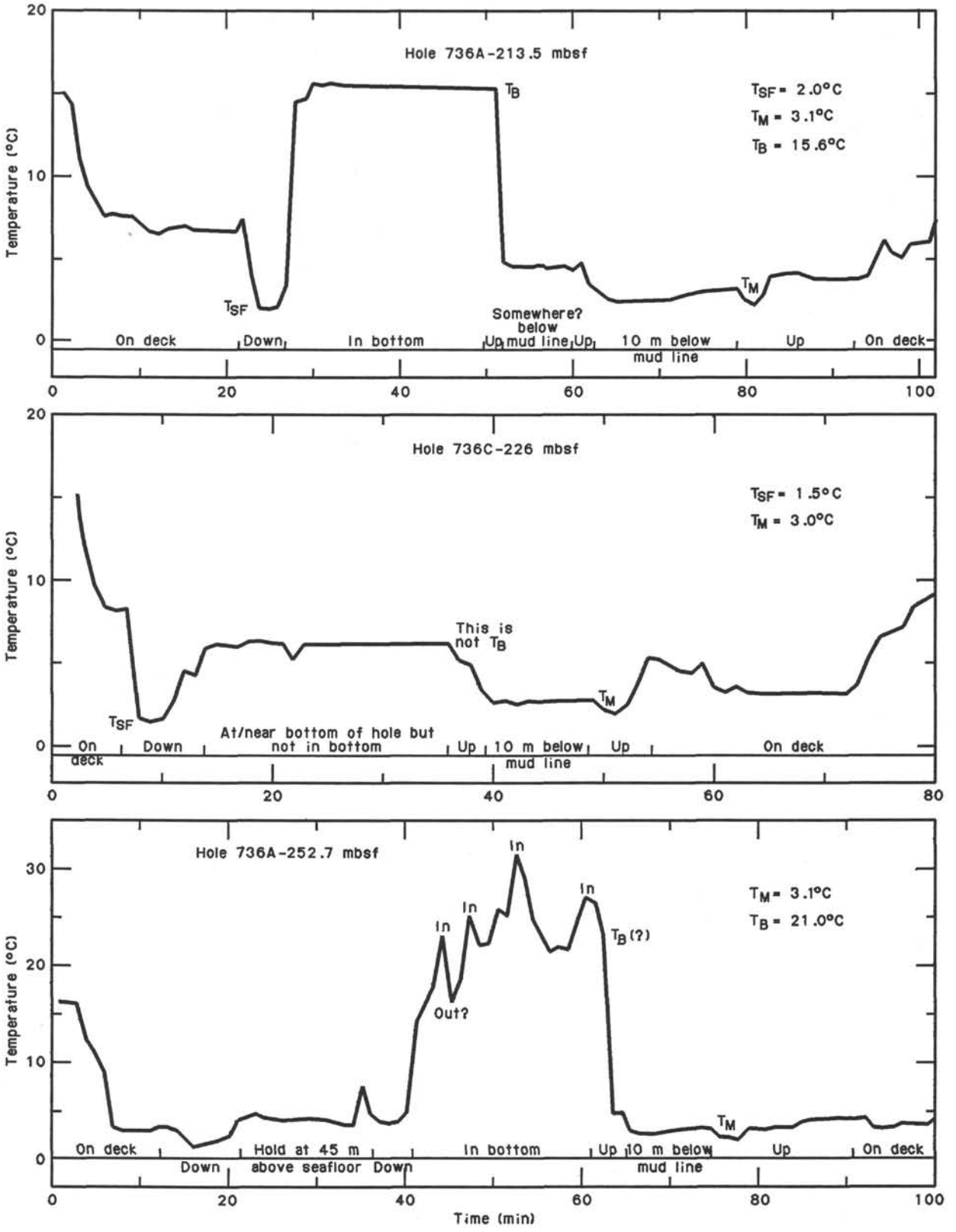

Figure 20 (continued).

Table 15. Temperature measurements for Site 736.

Core no.	Depth (mbsf)	Probe in sediment (min)	Probe equilibration time (min)	Temperature[a] (°C) T_{SF}	Temperature[a] (°C) T_B
119-736A-					
12H	79.5	17	12	1.5	6.2–7.1
18X	135.8	17	5	1.5	15.0–17.0
21H	164.4	21	19	1.6	17.9
26X	213.5	23	21	2.0	15.2
30X	252.7	20	8	?	18.4–20.5
119-736C-					
3R	226.0	0	0	1.5	—

[a] T_{SF} = lowest temperature immediately prior to probe penetration; T_B = equilibration temperature in sediment.

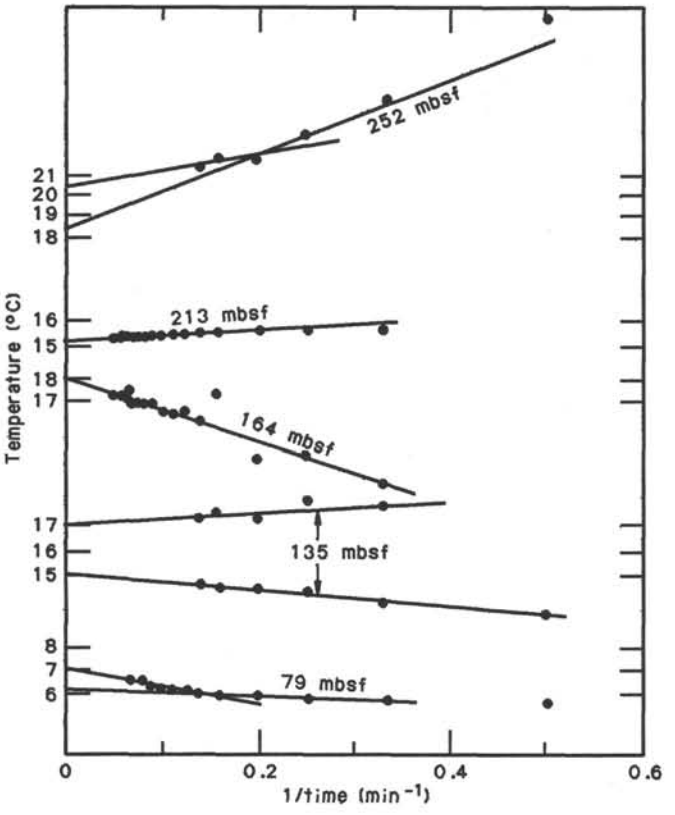

Figure 21. Temperature vs. 1/time, Hole 736A.

ture profile. Initial penetration of the probe into the sediment was attained for all depths except 226 mbsf in Hole 736C, where the probe apparently did not reach, or stay beneath, the sediment interface. Thin (about 0.3-m-thick) gravel layers were commonly recovered from the core tops directly following each temperature measurement. The gravel, derived from layers higher in the hole, did not prevent penetration but may explain some large frictional-heating temperature peaks upon insertion.

Temperatures are high in the upper 120 m of Hole 736A, increasing from about 1.6°C at the seafloor to 18°C at 164 mbsf. Temperatures then decrease about 3° over the next 50 m and finally increase to 18°–20°C at the deepest measurement (253 mbsf). The average temperature gradient in Hole 736A (seafloor to 253 mbsf) is about 70°C/km. The high temperature gradients for the predominantly diatomaceous sedimentary section at Site 736 are probably explained by the low thermal-conductivity values at this site.

The cause of the apparent decrease in temperatures from 164 to 215 mbsf is unknown. The equilibrium temperatures appear to be reliable. Increased conductivity values at these depths could cause smaller temperature gradients; however, conductivity increases would not explain a negative temperature gradient. A possible, but unconfirmed, explanation is heat transfer by circulation of pore fluids in the highly porous, and probably permeable, diatomaceous sediments.

The heat flow at Site 736 is estimated to be 52.8 W/m^2 (1.26 HFU), based on an average temperature gradient of 70°C/km and an average thermal conductivity of 0.75 W/m/°C. The observed temperature gradients, although high, may not reflect true heat flow because the high sedimentation rates since the late Pliocene (140 m/m.y.; "Biostratigraphy" section, this chapter) would have had a cooling effect. The high sedimentation rates may have decreased temperatures by 20% to 30% (i.e., true heat flow could be 20% to 25% higher than 58.5 W/m^2).

The estimated temperature at the bottom of the deepest hole at Site 736, 736C, based on downward projection of the 78°C/km temperature gradient in Hole 736A, is about 28°C at 371 mbsf.

In summary, good temperature measurements were obtained at five depths within the upper 253 mbsf at Site 736, giving an average temperature gradient of 70°C/km and a heat flow of 52.8 W/m^2 (1.26 HFU).

Discussion

Bulk densities for Site 736 are generally less, whereas water contents and porosities are usually higher, for a given depth and show less distinct trends with depth than for sediments at other high-latitude sites (e.g., ODP Sites 643, 689, and 690). This comparison is also true for trends in shear strength and compressional-wave velocity and probably results from (1) the more homogenous nature of the sequence at Site 736; (2) probable, overall higher biogenic silica content; and (3) possibly more extensive core disturbance.

In addition to showing anomalous index-property and shear-strength values and velocities in diatomaceous sediment, core disturbance in this sediment type is also clearly demonstrated at Site 736. Shear strength is the most obviously affected.

Comparison between different properties in the disturbed cores of Hole 736C shows some evidence of sediment structure. The fact that shear strengths drop to almost zero and the sediment appears soupy—whereas the water content and porosity decrease and bulk density remains constant—probably results from the diatom ooze having a strong framework that may be completely disrupted by drilling disturbance; in other words, the sediment liquifies. The apparent changes in index properties probably result from the escape of water from the remolded core prior to sampling.

SEISMIC STRATIGRAPHY

Munschy and Schlich (1987) used the seismic section MD 26-10 across Site 736 (target Site KHP-1) as an illustration of their seismic stratigraphy of the area; thus, the seismic correlation is clear (Figs. 22 and 23). Based on the results of the sonobuoy experiment (see "Site Geophysics" section, this chapter), the prominent unconformity reflector A is situated at approximately 825 mbsf. The top of the underlying sequence is locally truncated. According to Munschy and Schlich (1987) the unconformity marks a hiatus separating the middle Eocene from the lower Miocene and, thus, the pre-rifting sequence from the post break-up sediments, but the results from the site indicate a shorter duration of the hiatus. The nature of the unconformity is further discussed in the "Site 737" chapter.

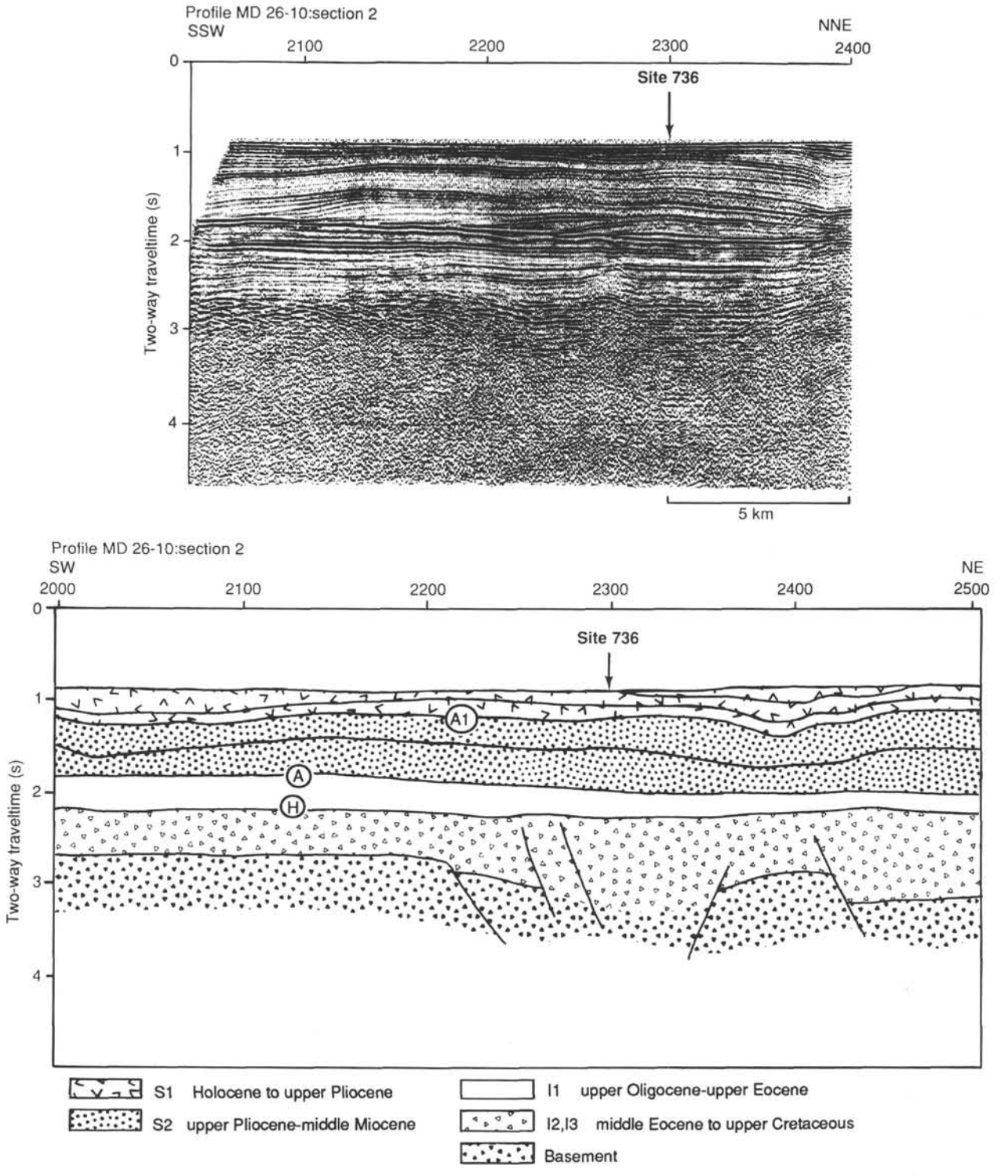

Figure 22. Multichannel seismic section across Site 736. Seismic line courtesy of R. Schlich; interpretation from Munschy and Schlich (1987). For detailed correlation with drilled section see "Site Geophysics" section. Location of line shown on Figure 1.

The seismic sequence above reflector A is divided into two units, S1 and S2, which Munschy and Schlich (1987) separated with reflector A1. A1 is at approximately 260 mbsf at Site 736. This corresponds closely with the boundary between lithologic Units I and II ("Lithostratigraphy and Sedimentology" section). In the multichannel seismic lines A1 appears as a fairly strong reflector with great continuity on top of a sheet drape that has a very light appearance on the records. On *JOIDES Resolution* single-channel seismic records A1 appears as the boundary between an upper sequence (S1) characterized by close parallel reflections and a lower sequence (S2) that is almost reflection free in its upper part.

The lower unit S2 in the area of Site 736 is characterized by 5- to 10-km-wide and 200- to 400-m-high mounds composed of sheet drape units, which appear as wavy but nearly concordant reflectors. The thickness of the individual sheets varies relatively

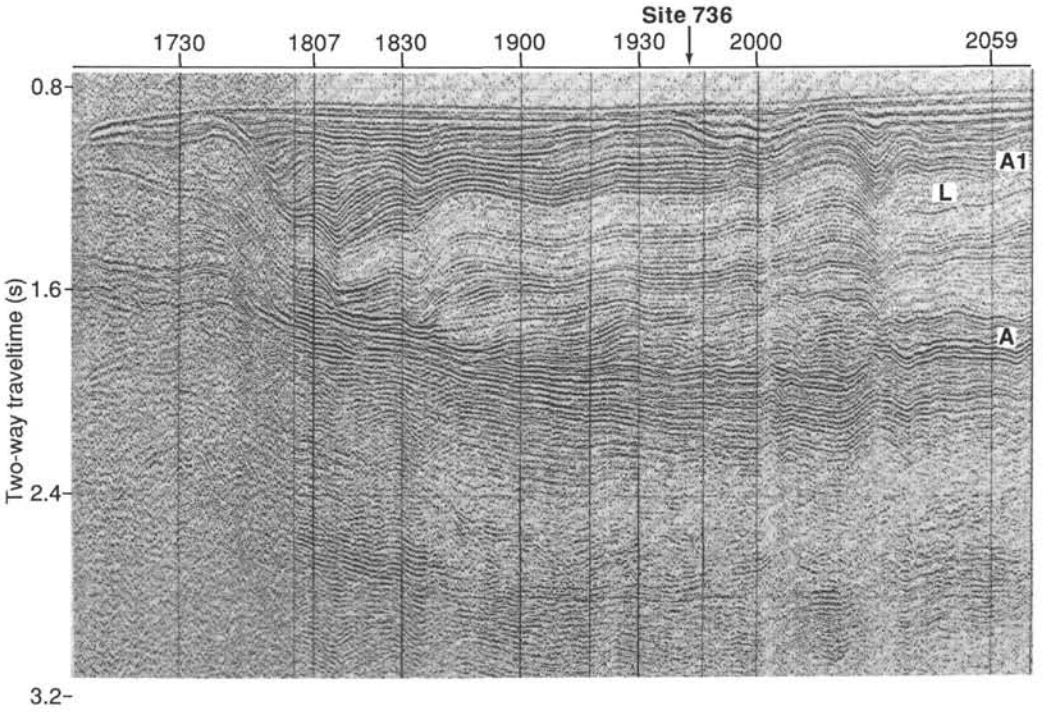

Figure 23. Single-channel seismic section made by *JOIDES Resolution* across Site 736 from north to northwest. Reflections designated according to Munschy and Schlich (1987). The light layer is marked L. The sequence above reflector A1 (also called S1) increases in thickness toward the north and fills in a channel? north of the mound. Location of line shown on Figure 1.

little horizontally even though the depths to the top of the sheets' surface (paleoseafloors) vary from 200 to 600 mbsf. The base of the mounds near reflector A is characterized by a series of downlaps into reflector A, which is formed by the bases of the sheets. Judging from the seismic lines, internal unconformities are not common inside of the mounds. The direction of the downlaps on the northern part of the plateau is chiefly, but not exclusively, toward north and upslope of reflector A. According to the isopach map of sequence A2 in Munschy and Schlich (1987), the big mound observed at the site is part of two long sediment ridges or drifts along the base of the insular shelf of the Kerguelen Plateau. The light layer mentioned previously seems to form an 80- to 100-m-thick uniform cover over the mound. Coring at Site 736 has documented that this cover consists of homogenous diatom ooze with almost no admixture of coarse terrigenous grains. This is suggestive of uniform pelagic sedimentation.

The upper unit S1 near Site 736 is characterized by a nearly parallel band of reflections. Lenticular bodies of low acoustic reflectivity are intercalated into this pattern. Coring penetrated one of these bodies between 85 and 110 mbsf, but no distinctive differences from the rest of the sedimentary sequences were recognized. However, it may be significant that the diatom ooze corresponding to seismic unit A1 contains mostly thin layers of sand and gravel, which probably cause the acoustic character of the sequence. North of the site, the individual reflection bands increase in thickness, forming a sequence of sigmoidal progradational bodies in the basin or channel north of the mound. Eventually, the channel is filled in by sediment bodies clearly prograding from the south. The whole of sequence A1 and A2 is unconformably covered with a relatively thin layer of presumably Holocene sediments, forming the relatively level surface of the recent bank. The sedimentation rate of this layer was probably lower than the rest of the sequence at Site 736 (see "Sedimentation Rates" section).

Conclusions

The older sequence above the unconformity (S2) seems to have been deposited as long sedimentary drift ridges formed by currents, which in the northern part of the ridge flowed northward along the slope of the Kerguelen insular shelf. The sedimentary ridge is locally up to 700 m thick, and no signs of erosion have been observed in the upper part. This suggests that the water depth was not less than 1000 m above the level of reflector A at the time of deposition. The covering light layer indicates a continuation of the pelagic type of sedimentation and a decrease in the influence of currents in the area.

The upper sequence is also mostly a pelagic diatom ooze, but an additional contribution from glacial-rafted material and possibly sporadic terrigenous mud flows is important. The sedimentary structures indicate that sediment transport from a southerly direction was dominant and that the depocenters were chiefly the local basins in the topography. Possible erosion occurred in the higher parts of the Kerguelen Plateau (e.g., Site 737), which is indicative that current transport has increased in importance relative to that of the previous stage. A decrease in water depth, tectonic tilting of the platform, and change of current pattern are possible causes.

SUMMARY AND CONCLUSIONS

Site 736 (49°24.12′S, 71°39.61′E) lies on the northern part of the Kerguelen-Heard Plateau in a water depth of 629 m. The 371-m-thick section cored at the site in three holes consists of upper lower Pliocene to Quaternary diatomaceous ooze with variable contributions from volcanic debris and very little carbonate. Sediment-accumulation rates range from 45 m/m.y.

above 80 mbsf (about 1.4 Ma) to 140 m/m.y. in the underlying interval to the extrapolated basal age of Hole 736C at 3.5 Ma. The sediments cored comprise a high-resolution biosiliceous reference section for the latest Cenozoic located near the present-day location of the Antarctic Convergence.

Lithostratigraphy

Two lithologic units are recognized in the sediments recovered from Site 736. The upper 257 m (Unit I) of section cored consists of diatomaceous ooze containing basaltic volcanic debris whereas the lower 114 m (Unit II) of the cored section is diatom ooze, which includes very little feldspathic detritus, pumice, and a thin layer of calcareous nannofossil ooze. These two units are also recognizable by seismic stratigraphy. The upper unit is characterized by tightly spaced reflections, and the lower unit displays more diffuse reflections. These seismic units are traceable regionally, and they probably correspond with seismic unit S1 and the upper part of unit S2 of Munschy and Schlich (1987), respectively. The upper unit shows considerable thickening and thinning in the nearby area, and it fills in hollows and covers the topography of the lower unit. The age of the base of Unit I is approximately 2.6 Ma according to diatom biostratigraphy, so the unit corresponds to the latest Cenozoic time of increased intensity of Antarctic glaciation. This age, the dispersed nature of pebble-sized clasts in the sediments, and the presence of faceting, striations, or a bullet-nosed shape of some of the pebbles argue for emplacement by ice rafting, possibly from glaciers on nearby Kerguelen Island.

Alternatively, some of the diatom ooze with incorporated volcanic detritus in Unit I may have been deposited by debris flows. Features supporting this mode of deposition include (1) sharp contacts with underlying purer diatom oozes that show basal size grading from some of the volcanic-bearing oozes; (2) incorporation of isolated bodies of volcanic-bearing ooze in other horizons, including in relatively pure ooze; (3) apparent post-depositional disturbance of bedding relations with locally subvertical boundaries; and (4) partial destruction of lithological boundaries, many of which are diffuse or wispy (cuspate). These debris flows could be redeposited glacially derived sediments that had accumulated higher on the plateau and closer to emergent areas. However, the upper unit displays a generally pelagic, draping relationship with underlying Unit II.

Biostratigraphy and Paleoclimatology

All of the cores taken at Site 736 contain common to abundant diatoms and radiolarians, and standard Antarctic zonations can be applied. Diatoms and radiolarians are generally well preserved, and little, if any, reworking of older species is observed. Deposition appears to have been continuous, and no hiatuses are present. The majority of the diatom species is typical of the Southern Ocean, but species more typical of middle latitudes are sporadically present, especially in the pre-uppermost Pliocene. Further study is required in order to determine times of movement of the Antarctic Convergence back and forth across the site. The radiolarian assemblage is notable because of the relatively low number of species (15 to 20) compared with Southern Ocean assemblages of equivalent age. This low diversity is probably due to the relatively shallow depositional depth of the site and the high amount of upwelling and surface-water productivity present.

The scarcity and low diversity of the calcareous nannofossil and foraminiferal assemblages in Site 736 sediments probably, in part, reflect the presence of strong upwelling and surface-water productivity at the site as well as the overall Antarctic aspect of the assemblages. Essentially no refined calcareous biostratigraphic zonations could be recognized. Palynomorphs are essentially barren from Site 736 sediments.

The magnetic signal of the Site 736 sediments is weak, and a magnetic reversal stratigraphy could not be established.

Chemistry

Most of the samples analyzed for interstitial waters contain $<5\%$ calcium carbonate and $<1\%$ organic carbon. The low amount of organic carbon could be further evidence of resuspension of the sediments by debris flows and transportation over short distances. The good quality of preservation of both the diatoms and the radiolarians and the scarcity of reworking argue against redeposition and transport by bottom currents over long distances.

Phosphate, silica, and ammonium are the only chemical species that show significant variations in their interstitial-water concentrations downhole at Site 736. Phosphate and ammonium decrease downsection, whereas silica concentrations increase and suggest the onset of silica diagenesis. Although much higher than the values found in seawater, dissolved phosphate and ammonium concentrations are considerably less than the values found in sediments beneath highly productive surface waters typified by upwelling (e.g., Peru margin; Suess, von Huene, et al., 1988).

The absence of hydrocarbon gases and the presence of sulfate in Site 736 sediment pore waters indicate that methanogenic bacteria have been inactive since the time of deposition. Organic carbon is high to moderate for diatomaceous sediments (1% in the upper 200 m of sediments), but the organic matter present is immature. The depositional environment of Site 736 has been aerobic, and the kerogen is mostly from varied sources, indicating reworking.

Physical Properties

The upper 235 m of the Site 736 sediment column shows an overall decrease in water content whereas porosity, bulk density, and grain density stay relatively constant. This unusual feature is probably a consequence of the lithology of diatom oozes, which tend to maintain a relatively open but strong structure downcore. Measurements of shear strength and compressional-wave velocity are strongly affected by coring disturbance caused by XCB and RCB coring below about 110 mbsf, but they show an increase with depth above that horizon.

Heat Flow

The heat flow at Site 736 is estimated to be 52.8 W/m^2 (1.26 HFU), based on measured downhole temperatures, which suggest a temperature gradient of 70°/km and average thermal conductivities of 0.75 W/m/°C. The estimated temperature at the bottom of Hole 736C is 28°C.

REFERENCES

Barker, P. F., and Burrell, J., 1982. The influence upon Southern Ocean circulation, sedimentation, and climate of the opening of Drake Passage. *Antarct. Geosci.*, B(4):377–385.

Barker, P. F., Kennett, J. P., et al., 1988. *Proc. ODP, Init. Repts.*, 113: College Station, TX (Ocean Drilling Program).

Brewster, N. A., 1980. Cenozoic biogenic silica sedimentation in the Antarctic Ocean, based on two Deep Sea Drilling sites. *Geol. Soc. Am. Bull.*, 91:337–347.

Caulet, J. P., 1986. A refined radiolarian biostratigraphy for the Pleistocene of the temperate Indian Ocean. *Mar. Micropaleontol.*, 11:217–229.

Chen, P. H., 1975. Antarctic radiolaria. *In* Hayes, D. E., Frakes, L. A., et al., *Init. Repts. DSDP*, 28: Washington (U.S. Govt. Printing Office), 437–513.

Ciesielski, P. F., 1983. The Neogene and Quaternary diatom biostratigraphy of subantarctic sediments, Deep Sea Drilling Project Leg 71. *In* Ludwig, W. J., Krasheninnikov, V. A., et al., *Init. Repts. DSDP*, 71: Washington (U.S. Govt. Printing Office), 635–665.

Ciesielski, P. F., and Grinstead, G. P., 1986. Pliocene variations in the position of the Antarctic Convergence in the southwest Atlantic. *Paleoceanography*, 1:197–232.

Clark, S. P., 1966. Handbook of physical constants. *Mem. Geol. Soc. Am.*, 97.

Claypool, G. E., and Kvenvolden, K. A., 1983. Methane and other hydrocarbon gases in marine sediments. *Annu. Rev. Earth Planet. Sci.*, 11:299–327.

Deroo, G., Herbin, J. P., Roucache, J. R., and Tissot, B., 1979. Organic geochemistry of Cretaceous mudstones and marly limestones from DSDP Sites 400 and 402, Leg 48, eastern North Atlantic. *In* Montadert, L., Roberts, D. G., et al., *Init. Repts. DSDP*, 48: Washington (U.S. Govt. Printing Office), 921–930.

Deroo, G., Herbin, J. P., Roucache, J. R., Tissot, B., Albrecht, P., and Dastillung, M., 1978. Organic geochemistry of some Cretaceous claystones from Site 391, Leg 44, western North Atlantic. *In* Benson, W. E., Sheridan, R. E., et al., *Init. Repts. DSDP*, 44: Washington (U.S. Govt. Printing Office), 593–598.

Echols, R. J., 1971. Distribution of foraminifera in sediments of the Scotia Sea, Antarctic waters. *Antarctic Res. Ser.*, 15:93–168.

Eldholm, O., Thiede, J., et al., 1987. *Proc. ODP, Init. Repts.*, 104: College Station, TX (Ocean Drilling Program).

Frohlich, F. A., 1983. MD 35/DRAKAR á bord du *Marion Dufresne*, 1 Mars-Avril 1983. *Miss. Rech. Terr. Austr. et Antarct. Franc., Rapp. Camp. Mer.*, 83-2:1–97.

Fryxell, G. A., and Kendrick, G. A., 1988. Austral spring microalgae across the Weddell Sea ice edge: spatial relationships found along a northward transect during AMERIEZ 83. *Deep-Sea Res., Part A*, 35:1–20.

Gieskes, J. M., Elderfield, H., Lawrence, J. R., Johnson, J., Meyers, B., and Campbell, A., 1982. Geochemistry of interstitial waters and sediments, Leg 64, Gulf of California. *In* Curray, J. R., Moore, D. G., et al., *Init. Repts. DSDP*, 64: Washington (U.S. Govt. Printing Office), 675–694.

Gordon, A. L., 1971. Oceanography of Antarctic waters. *In* Reid, J. L. (Ed.), *Antarctic Oceanology, 1*: Antarctic Res. Ser., 15:169–204.

Kemp, E. M., Frakes, L. A., and Hayes, D. E., 1975. Paleoclimatic significance of diachronous biogenic facies, Leg 28, Deep Sea Drilling Project. *In* Hayes, D. E., Frakes, L. A., et al., *Init. Repts. DSDP*, 28: Washington, (U.S. Govt. Printing Office), 909–917.

Kennett, J. P., and Srinivasan, M. S., 1983. *Neogene Planktonic Foraminifera*: Stroudsburg, PA (Hutchinson Ross).

Krauskopf, K. B., 1956. Dissolution and precipitation of silica at low temperatures. *Geochim. Cosmochim. Acta*, 10:1–26.

Lachenbruch, A. H., and Marshall, B. V., 1966. Heat flow through the Arctic Ocean floor: the Canada Basin–Alpha Rise boundary. *J. Geophys. Res.*, 71:1223–1248

Leclaire, L., 1983. *MD 48, Marion Dufresne, NASKA Oceanographic Cruise on the Kerguelen Plateau: Piston Core and Dredge Localities, Descriptions*: Paris (Museum National d'Historie Naturelle, Laboratorie de Geologie).

Lindenberg, H. G., and Auras, A., 1984. Distribution of arenaceous foraminifera in depth profiles on the Southern Ocean (Kerguelan Plateau area). *Palaeogeogr. Palaeoclimatol. Palaeoecol.*, 48:61–106.

Matsuda, J., and Von Herzen, R. P., 1986. Thermal conductivity variation in a deep-sea sediment core and its relation to water, Ca and Si content. *Deep-Sea Res., Part A*, 33:165–175.

Munschy, M., and Schlich, R., 1987. Structure and evolution of the Kerguelen-Heard Plateau (Indian Ocean) deduced from seismic stratigraphy studies. *Mar. Geol.*, 76:131–152.

Nougier, J., 1970. Contribution à l'étude géologique et géomorphologique des iles Kerguelen. *Com. Nat. Fr. Rech. Antarct.*, 27:1–440.

Schlich, R., and Leclaire, L., 1981. *MD 26—Oceanographic Cruises on the Kerguelen-Heard Plateau: Piston Core and Dredge Locations, Piston Core Descriptions*: Paris (Museum Nationale d'Historie Naturelle, Laboratorie de Geologie).

_____, 1983. *MD 35—Oceanographic Cruises on the Kerguelen-Heard Plateau: Piston Core and Dredge Locations, Piston Core Descriptions*: Paris (Museum Nationale d'Historie Naturelle, Laboratorie de Geologie).

Shipboard Scientific Party, 1988. Site 695. *In* Barker, P. F., Kennett, J. P., et al., *Proc. ODP, Init. Repts.*: College Station, TX (Ocean Drilling Program), 527–606.

Stow, D.A.V., and Piper, D.J.W. (Eds.), 1984. Fine-Grained Sediments: Deep Water Processes and Facies: *Spec. Publ. Geol. Soc. London.*

Stumm, W., and Morgan, J. J., 1970. *Aquatic Chemistry*: New York (Wiley).

Suess, E., von Huene, R., et al., 1988. *Proc. ODP, Init. Repts.*, 112: College Station, TX (Ocean Drilling Program).

Tissot, B. P., and Welte, D. H., 1984. *Petroleum Formation and Occurrence* (2nd ed.): Berlin (Springer-Verlag).

Weaver, F. M., 1983. Cenozoic radiolarians from the southwest Atlantic, Falkland Plateau region, Deep Sea Drilling Project Leg 71. *In* Ludwig, W. J., Krasheninnikov, V. A., et al., *Init. Repts. DSDP*, 71: Washington (U.S. Govt. Printing Office), 667–686.

Ms 119-104